Targeting the dependence on PIK3C3-mTORC1 signaling in dormancy-prone breast cancer cells blunts metastasis initiation

Authors

Islam E. Elkholi[1,2,*], Amélie Robert[1], Hellen Kuasne[3], Stanislav Drapela[4], Graham Macleod[5,6], Steven Hébert[7], Alain Pacis[3,8], Virginie Calderon[1], Claudia L. Kleinman[7,9], Ana P. Gomes[4], Julio A. Aguirre-Ghiso[10-13], Morag Park[3,†], Stéphane Angers[5,6,14,†], Jean-François Côté[1,2,15,16,*]

Affiliations

[1]Montreal Clinical Research Institute, Montreal, Canada.
[2]Molecular Biology Programs, Université de Montréal, Canada.
[3]Rosalind and Morris Goodman Cancer Institute, McGill University, Canada.
[4]Department of Molecular Oncology, H. Lee Moffitt Cancer Center & Research Institute, Tampa, USA.
[5]Donnelly Centre for Cellular & Biomolecular Research, University of Toronto, Canada.
[6]Leslie Dan Faculty of Pharmacy, University of Toronto, Canada.
[7]Lady Davis Institute for Medical Research, Jewish General Hospital, Montreal, Canada.
[8]Canadian Centre for Computational Genomics, McGill University, Montreal, Canada.
[9]Department of Human Genetics, McGill University, Canada.
[10]Department of Cell Biology, Albert Einstein College of Medicine, Bronx, USA.
[11]Cancer Dormancy and Tumor Microenvironment Institute, Albert Einstein Cancer Center, Albert Einstein College of Medicine, Bronx, USA.
[12]Ruth L. & David S. Gottesman Institute for Stem Cell Research & Regenerative Medicine, Albert Einstein Cancer Center, Albert Einstein College of Medicine, Bronx, USA.
[13]Institute for Aging Research, Albert Einstein Cancer Center, Albert Einstein College of Medicine, Bronx, USA.
[14]Department of Biochemistry, Temerty Faculty of Medicine, University of Toronto, Canada.
[15]Department of Biochemistry and Molecular Medicine, Université de Montréal, Canada.
[16]Department of Anatomy and Cell Biology, McGill University, Canada.

[†] denotes equal contribution.

[*] Corresponding authors:

Islam E. Elkholi, MD, PhD

Montreal Clinical Research Institute (IRCM),
110 Pine Ave West, Montreal,
Québec, H2W1R7 Canada.
Email : islam.elkholi@mail.mcgill.ca
Phone: 514 987-5656

Jean-François Côté, PhD

Montreal Clinical Research Institute (IRCM),
110 Pine Ave West, Montreal,
Québec, H2W1R7 Canada.
Email : jean-francois.cote@ircm.qc.ca
Phone: (514) 987-5647

Abstract

Halting breast cancer metastatic relapses following primary tumor removal and the clinical dormant phase, remains challenging, due to a lack of specific vulnerabilities to target during dormancy. To address this, we conducted genome-wide CRISPR screens on two breast cancer cell lines with distinct dormancy properties: 4T1 (short-term dormancy) and 4T07 (prolonged dormancy). We discovered that loss of class-III PI3K, Pik3c3, revealed a unique vulnerability in 4T07 cells. Surprisingly, dormancy-prone 4T07 cells exhibited higher mTORC1 activity than 4T1 cells, due to lysosome-dependent signaling occurring at the cell periphery. Pharmacological inhibition of Pik3c3 counteracted this phenotype in 4T07 cells, and selectively reduced metastasis burden only in the 4T07 dormancy prone model. This mechanism was also detected in xenografts from human breast cancer patients, supporting that it may be relevant in humans. Our findings suggest dormant cancer cell-initiated metastasis may be prevented in patients carrying tumor cells that display PIK3C3-peripheral lysosomal signaling to mTORC1.

Teaser

PIK3C3-mTORC1 signaling is a novel druggable pathway in breast cancer metastasis.

INTRODUCTION

Nearly one-quarter of breast cancer patients present with a metastatic relapse within months to as long as 20 years after the diagnosis and management of their primary tumors (*1-3*). This is attributed to the phenomenon of metastatic dormancy, whereby tumor cells homing to secondary sites within the body enter a state of quiescence (i.e., cellular dormancy) and/or balanced proliferation and apoptosis (i.e., micrometasatatic dormancy) that collectively lead to metastatic disease that is undetectable by current tests. Although this notion is well recognized, the molecular and biological dynamics underlying metastatic dormancy is still in its infancy (*4*). Understanding the molecular determinants behind the switch from dormancy to metastatic outgrowth in addition to the survival mechanisms of dormant disseminated tumor cells (DTCs) is needed to develop effective therapeutic approaches for preventing relapse. Currently such molecular determinants can be categorized into two independent, yet inseparable factors: cancer cell intrinsic factors and microenvironmental cues that can direct the fate and response of DTCs to therapies (*5-8*).

Different human and murine breast cancer cell line models that share an origin but differ in metastatic behavior have been leveraged to explore the determining factors of the fate of DTCs (reviewed in (*8*)). A widely used model is the 4T1 and 4T07 murine breast cancer cell line pair that originated from a spontaneous metastatic nodule in BALB/c mice (*9*). In immunocompetent BALB/c mice, spontaneously disseminated 4T1 cells can form overt metastases in the lungs with a short latency period, while 4T07 cells remain dormant and show ultra-low frequency of metastasis. Interestingly, implanting 4T07 cells in immunocompromised (i.e. T-cell deficient) mice allow them to escape dormancy and develop overt metastases, but at a notable lower magnitude than the 4T1 cells (*10*). This clearly supports the notion that the two cell lines are intrinsically different. Indeed, investigating the differentially expressed genes between 4T1- and 4T07-based primary tumors identified TWIST1 as a gene elevated in 4T1 cells mediating epithelial-mesenchymal transition and high metastatic burden (*11*). In addition, a gain-of-function screen using a 4T1-derived cDNA library identified Coco as a mediator of reactivation of dormant 4T07 cells in the lungs (*12*). A third study demonstrated that 4T1 tumors and cells *in vitro*, in comparison to 4T07 counterparts, express higher levels of Cxcl1 that enables the former to promote more neutrophil extracellular traps (NETs) and hence higher ability to generate overt metastases (*13*). Thus, studying these two cell lines in parallel offers an opportunity to explore new aspects of cancer cell intrinsic factors that contribute to metastatic progression and/or response to therapeutic intervention.

Here, we asked whether 4T1 and 4T07 cells exhibit differential activity in signaling pathways that could be exploited for therapeutic intervention *in vivo*. We harnessed a genome wide loss-of-function CRISPR screening-based framework (*14, 15*) to systematically reveal the fitness genes that 4T1 vs. 4T07 differentially depend on for growth. Identifying the fitness genes that contribute to a specific signaling pathway not only indicates the potential activity of the pathway but also suggests the sensitivity of cells to targeted inhibition of the pathway (*14, 16, 17*). We discovered that 4T1 cells, but not 4T07 cells, depend on and display higher activity of class I PI3K, and accordingly, are more sensitive to pharmacological inhibition of this pathway. However, counterintuitively, we discovered that the 4T07 cells demonstrate higher activity of the downstream mechanistic Target of Rapamycin complex 1 (mTORC1). Mechanistically, we show that 4T07 cells, but not 4T1 cells, depend on class III PI3K to mediate a constant peripheral lysosomal positioning that is linked to mTORC1 hyperactivity. This lysosome positioning-associated PIK3C3-mTORC1 signaling circuit is also observed in a patient-derived xenograft

104 (PDX) cell line originating from a patient diagnosed with breast cancer metastatic relapse.
105 Importantly, selective inhibition of PIK3C3 exclusively kills dormancy prone 4T07 cells.
106 Collectively, our data suggest that the PIK3C3-mTORC1 signaling axis may be a druggable target
107 to alleviate metastatic burden in breast cancer patients by eliminating disseminated cancer cells.

RESULTS

Genome-wide knockout CRISPR screens define differential fitness genes in 4T1-4T07 cells

We first aimed at characterizing the molecular subtype of breast cancer modeled by the 4T1-4T07 cells. We generated and correlated RNA-Seq transcriptomic data from these two cell lines with gene expression data from 47 human breast cancer cell lines. We conclude that 4T1-4T07 are closer to the human basal B molecular breast cancer subtype predominantly within the triple negative clinical breast cancer subtype, complementing a recent investigation of 4T1 cells (*18*) (Fig. S1; Table S1). The 4T07 cells also display features of the basal B subtype consistent with a common origin of the 4T1 and 4T07 cells (Fig. S1; Table S1).

Genome-wide loss-of-function CRISPR screens enable the identification of core and context-dependent fitness genes, revealing common and specific active signaling nodes (*14, 15, 19*). Fitness genes are those that when perturbed result in a proliferative or survival disadvantage for cells. Therefore, it is plausible that 4T1-specific fitness genes are candidate survival or metastatic progression mediators. Meanwhile, 4T07-specific fitness genes might be candidate regulators of survival during dormancy or proliferation when implanted in permissive hosts or microenvironments. To explore these gene categories, we applied a CRISPR screening pipeline to 4T1-4T07 cells to uncover their differential fitness genes, and by extension, their differentially active signaling pathways. To this end, 4T1 and 4T07 cells were independently infected with the mGeCKO library, encompassing ~70,000 gRNAs targeting ~21,000 murine genes (*20*). Following selection for cells with gRNA integration (T0), genomic DNA was extracted at 3 consecutive timepoints over 3 weeks (T1, T2, and T3) to map gRNAs representation relative to T0. The BAGEL algorithm was used to identify the fitness genes of each cell line (Fig. 1A). Prior to downstream analysis, we performed a series of quality control analyses (Fig. S2). An adequate library coverage was verified in all samples (Fig. S2A-B). In addition, a distance correlation analysis demonstrated clustering of the screens' biological replicates as expected (Fig. S2C-D). Next, as a measure for the screen sensitivity, we calculated precision-recall curves using previously annotated lists of gold-standard essential and non-essential genes (Fig. S2E-F). Both the 4T1 and 4T07 screens showed high performance, with the BAGEL algorithm being able to discriminate essential from nonessential genes with high precision. As a final indicator of the robustness, fold-change distributions of gRNAs targeting essential genes, over the course of the screens, were prominently shifted while those targeting nonessential genes showed minimal change (Fig. S2G-H). Collectively, these analyses provided confidence in the ability of the performed screens to reveal fitness genes of the two cell lines.

In total, we identified 2014 and 2038 fitness genes in the 4T1 and 4T07 cells, respectively (see Methods for details). Merging the 4T1 and 4T07 screens defined 1257 common fitness genes between these cell lines (Fig. 1B; Table S2), that had enrichment for the same biological functions of previously annotated core essential genes (*14, 21*) (Fig. S3). 757 and 781 specific fitness genes were identified in 4T1 and 4T07, respectively (Fig. 1B; Table S3-4). Next, we focused on our goal of revealing differential signaling pathways dependencies between the two cell lines. Among top ranking 4T1-specific fitness genes were *Pik3ca*, encoding the catalytic subunit of the class-I PI3K, and *Rictor*, the core component of mTOR complex 2 (mTORC2) (Fig. 1C). Both genes act as positive regulators of the PI3K pathway (Fig. 1D). In contrast, some of the pathway's negative regulators (*Pten*, *Tsc1*, *Tsc2*, and *Pras40*) were identified as proliferation suppressor genes, whose

155 gRNAs were enriched at the last timepoint (T3) in reference to T0, in 4T1 cells (Fig. 1D and Table
156 S5). These data suggested that 4T1 cells may possess higher PI3K-AKT activity in comparison to
157 4T07 cells. To investigate whether this observation is reflected in the global transcriptome of the
158 two cell lines, we leveraged the RNA-sequencing dataset to perform a GSEA analysis that indeed
159 identified elevation of *AKT* and downregulation of *PTEN* gene signatures to be enriched in 4T1 in
160 comparison to 4T07 cells (Fig. 1E-F). By analyzing the 4T07-specific fitness genes, we identified
161 *Pik3c3*, encoding the catalytic subunit of the class-III PI3K, and its regulatory subunit *Pik3r4* (Fig.
162 1C). Given the clinical significance of the canonical class I PI3K pathway and the poorly explored
163 class III PI3K pathway in breast cancer, we sought to further investigate the differential
164 dependency on these PI3K classes.
165

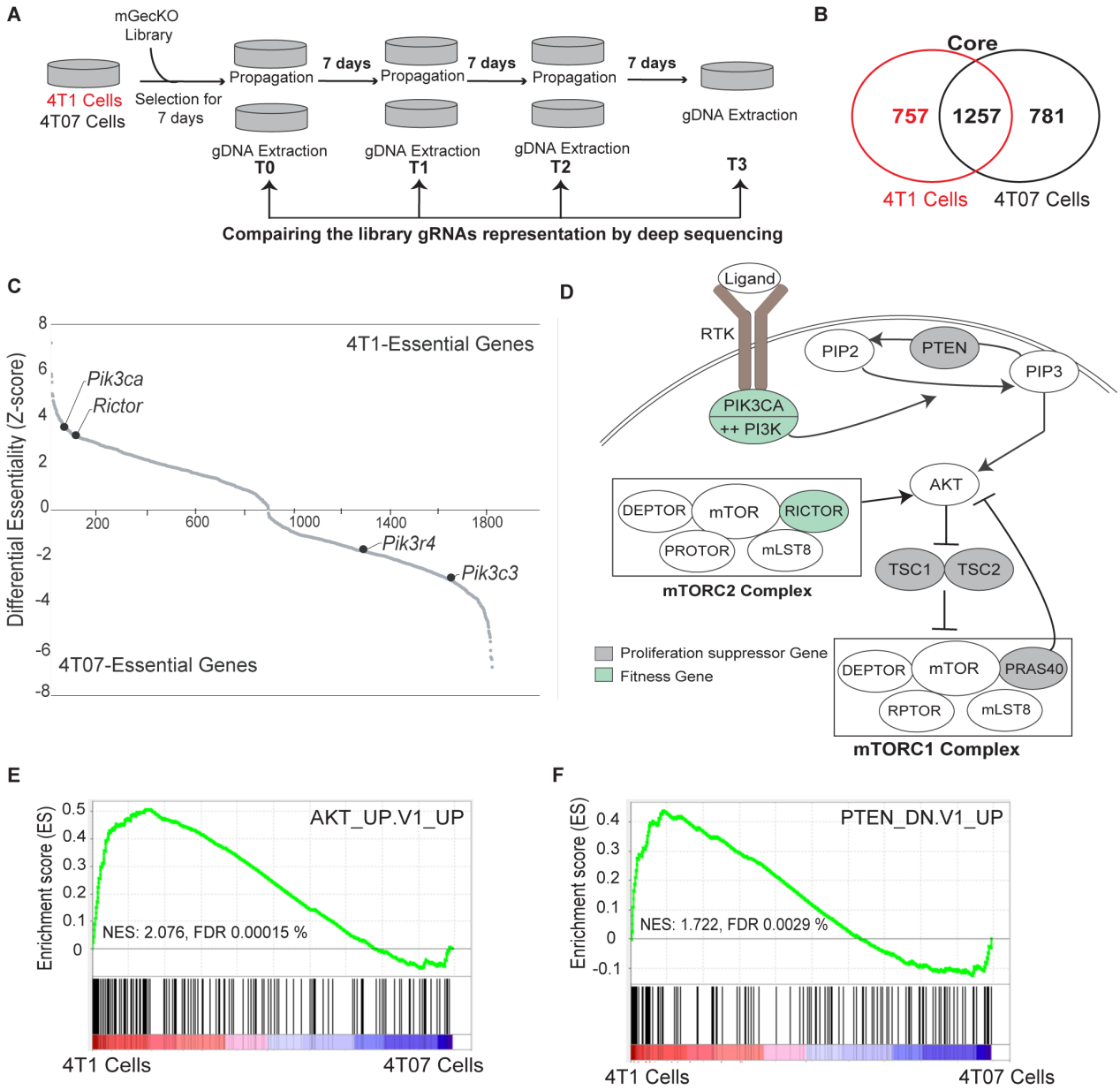

Figure 1

Figure 1. Genome-wide knockout CRISPR screens define the common and differential fitness genes in the 4T1-4T07 cells. (A) Schematic outline for the performed screens' pipeline. **(B)** Enumeration of the revealed cell line-specific and common fitness genes. **(C)** Ranked differential gene fitness score between the 4T1 and 4T07 cells. Value > 0 denotes 4T1-specific fitness gene; value < 0 denotes 4T07-specific fitness gene. **(D)** Schematic representation integrating the 4T1-specific fitness (in green) and proliferation suppressor genes (positively selected genes; in grey) in the canonical PI3K-AKT pathway. **(E-F)** GSEA analysis comparing the enrichment of genes previously found to be induced by AKT upregulation **(E)** or PTEN downregulation in the two cell lines **(F)**.

178 **Validation of *Pik3ca* and *Pik3c3* as differential fitness genes for 4T1 and 4T07 cells**

179

180 To validate the essentiality of *Pik3ca* in 4T1 cells, we performed a two-color competition assay
181 (*22*). 4T1 cells expressing Cas9 were generated and independently infected with either a vector
182 expressing a *Pik3ca*-targeting gRNA and GFP, or a vector expressing a gRNA targeting the
183 *Rosa26* locus and mCherry (Fig. 2A). The generated cell lines (green *Pik3ca* gRNA- and red
184 *Rosa26* gRNA-expressing cells) were co-cultured in a 1:1 ratio and the percentage of the green
185 population over total population was monitored for 10 passages (Fig. 2A). As predicted from the
186 CRISPR screen results, cells expressing the *Pik3ca* gRNAs significantly dropped out in
187 comparison to the control condition expressing the *Rosa26* gRNA (Fig. 2B-C). Next, a
188 complementary pharmacological validation approach revealed that treating 4T1 and 4T07 cells
189 with the PIK3CA-specific inhibitor BYL719 (*23*) significantly halted 4T1 cell proliferation
190 without affecting that of 4T07 cells (Fig. 2D). Next, we investigated the effect of Akt inhibition
191 on the two lines. As anticipated, the AKT inhibitor MK-2206 halted the proliferation of 4T1 cells
192 in a more prominent manner than 4T07 cells (Fig. 2E).

193

194 We next validated the essentiality of *Pik3c3* in 4T07 cells using the same two-color competition
195 assay (Fig. 2A). 4T07 cells expressing gRNAs targeting either *Pik3c3* or its binding partner *Pik3r4*
196 (also revealed in the screen) robustly dropped out throughout consecutive timepoints of the assay
197 (Fig. 2F-G). Meanwhile, a modest effect was noticed in the 4T1 cells (Fig. S4A-B). Indeed,
198 comparing the representation of *Pik3c3* gRNA-expressing 4T1 and 4T07 populations after
199 normalization to their respective control conditions (*Rosa26* gRNA-expressing cells) highlighted
200 the differential dependence on *Pik3c3* (Fig. S4C), as predicted by the fitness screens (Fig. 1C). We
201 then used a complementary pharmacological approach to directly assess whether inhibiting the
202 catalytic activity of Pik3c3 affects the survival of the two cell lines differentially. 4T07 and 4T1
203 cells were seeded and cultured on basal membrane extract (BME) where they form spheroids, then
204 VPS34IN1, a PIK3C3-specific inhibitor (*24*), was added at two different doses (5 uM and 10 uM)
205 and cell death rates were assessed (Fig. 2H). VPS34IN1 treatments led to a 2- to 3-fold increase
206 in death rate of 4T07 cells, with no significant effect on the 4T1 cells in reference to vehicle-
207 treated conditions (Fig. 2I-J). These two approaches suggest that Pik3c3 is indispensable for 4T07
208 cells in contrast to the 4T1 counterpart.

209

210 Altogether, these data demonstrate the differential dependence on PI3K classes in 4T1 and 4T07
211 cells was further extended to differential vulnerability towards specific inhibitors for these PI3Ks.
212 This prompted us to investigate whether these phenotypes are explained by differential signaling
213 activity in the PI3K-AKT-mTORC1 pathway.

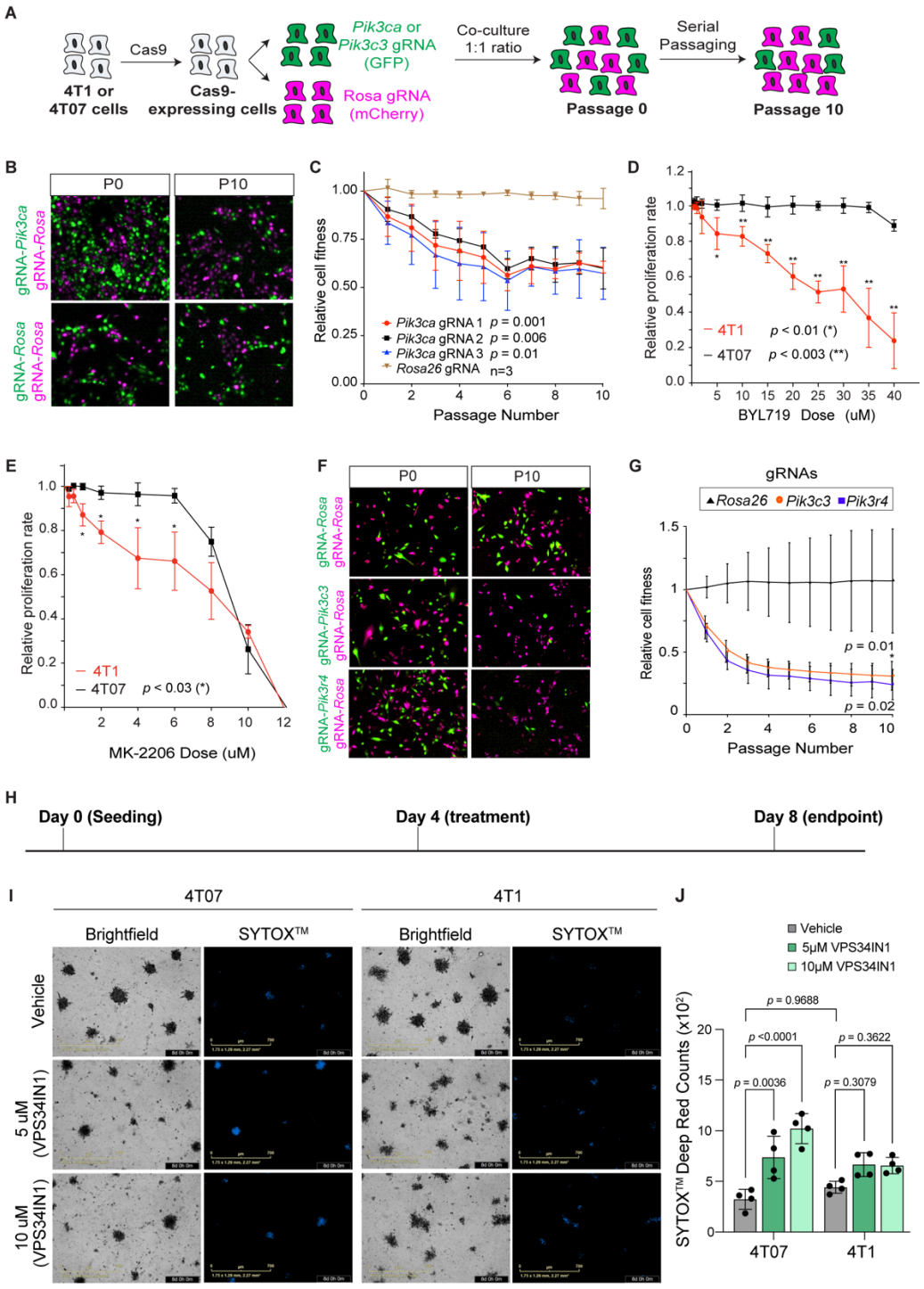

214 **Figure 2**

215 **Figure 2**. ***Pik3ca* and *Pik3c3* are differential fitness genes for the 4T1 and 4T07 cells. (A)**
216 Schematic representation for the two-color competition assay. **(B)** Representative images showing
217 either 4T1 cells expressing *Pik3ca*-gRNA or *Rosa26*-gRNA (both in green) co-cultured
218 independently with 4T1 cells expressing *Rosa26*-gRNA in magenta, at passages zero (P0) and 10
219 (P10). **(C)** Graph showing representation of the green 4T1 cell populations over serial passages in
220 reference to P0. **(D)** Proliferation assay comparing the 4T1-4T07 cells' response to BYL719. **(E)**
221 Proliferation assay comparing the 4T1-4T07 cells' response to MK-2206. **(F)** Representative
222 images showing either 4T07 cells expressing *Pik3c3*-gRNA, *Pik3r4*-gRNA, or *Rosa26*-gRNA (all

223 in green) co-cultured independently with cells expressing *Rosa26*-gRNA in magenta at passages
224 zero (P0) and 10 (P10). **(G)** Graph showing representation of the green 4T07 cell populations over
225 serial passages in reference to P0. **(H)** Schematic for the timeline of assessing the effect of
226 VPS34IN1 on the 4T07 and 4T1 cells' survival in (I-J). **(I)** Representative images of 4T07 and
227 4T1 3D spheroids at the experimental endpoint after treatment with either the vehicle (DMSO) or
228 VPS34IN1 at 5 uM and 10 uM. **(J)** Quantifications of cell death burden as indicated by positive
229 staining for SYTOX™.
230

231 **mTORC1 is differentially regulated in the 4T1 vs. 4T07 cells with higher activity in the 4T07**
232 **cells**

233

234 We assessed the activity of canonical downstream components of the PI3K pathway. In line with
235 the prediction from the genetic screens, 4T1 cells showed higher PI3K activity in untreated
236 conditions, as assessed by phosphorylated Akt levels (Fig. 3A-C). Furthermore, short-term
237 treatments with BYL719 (a selective PIK3CA inhibitor) inhibited the Pi3k-Akt-mTORC1
238 pathway to a similar extent in both cell lines, as demonstrated by reduced levels of phosphorylated
239 Akt, S6k1, and S6 (Fig. 3A). Next, we investigated the effect of short-term Akt inhibition and
240 found that it did not lead to the same effects as Pik3ca inhibition (Fig. 3B). In particular, mTORC1
241 activity, as assessed by phospho-S6k1 levels, was reduced upon inhibiting Akt only in 4T1 cells.
242 Prominently in the untreated conditions in both experiments (Fig. 3A-B), 4T07 cells demonstrated
243 two-fold higher mTORC1 activity than 4T1 cells (Fig. 3C), despite the dispensability and low
244 activity of the class I Pi3k in 4T07 cells (Fig. 3A-C). Such an intriguing finding was of interest
245 from a signaling and biological perspective for three reasons. First, the well-established feedback
246 loop between mTORC1 activity and response to PI3K inhibition (*25, 26*). Notably, sustained, or
247 reactivated, mTORC1 activity is a mechanism of resistance to the BYL719 (*25, 26*). Second,
248 PIK3C3, that we validated as a 4T07-specific fitness gene (Fig. 2F-J), mediates mTORC1 activity
249 specially when class I PI3K is inhibited for prolonged periods (*27*). Third, high mTORC1 activity
250 is a survival mechanism for dormant cells *in vivo* (*28*), but the mechanisms behind this have not
251 been resolved. Therefore, we set out to further dissect the previously unexplored mTORC1 activity
252 regulation in the 4T1 and 4T07 cells considering these observations.

253

254 We investigated the extent of dependence of each cell line on the class I Pi3k in mediating
255 mTORC1 activity. A low-dose of BYL719 (1 uM), under serum starvation or subsequent insulin
256 stimulation, reduced mTORC1 activity preferentially in 4T1 over 4T07 cells (Fig. S5A-C),
257 suggesting an incomplete dependence of 4T07 cells on class I Pi3k in regulating mTORC1. We
258 then tested whether the mTORC1 hyperactivity observed in 4T07 cells contributes to their poor
259 responsiveness to BYL719 treatment. 4T07 cells were treated with a high dose of BYL719 (10
260 uM) that did not affect their proliferation (Fig. 2D), and mTORC1 activity was measured after
261 short-term (2 hours) or long-term (24, 48, and 72 hours) treatments to mimic the proliferation
262 assay conditions (tested in Fig. 2D). We observed that mTORC1 activity started to increase after
263 48 hours of treatment (Fig. S5D). These findings suggested non-canonical regulation of mTORC1
264 in 4T07 cells.

265

266 Since gene essentiality and the mirrored activity of signaling pathways can be a consequence of
267 genomic alterations in driver oncogenes or tumor suppressor genes, we asked whether the
268 observed differences between the 4T1 and 4T07 cells could be explained by the genomic status of
269 genes involved in the Pi3k-Akt-mTORC1 pathway. To this end, we performed whole-genome
270 sequencing (WGS) on the 4T1 and 4T07 cell lines in reference to genomic DNA extracted from a
271 mammary fat pad of a female BALB/c mouse. Despite the high sequencing coverage (see
272 Supplementary Methods), no differential genomic alterations of established functional
273 consequences in the Pi3k-Akt-mTORC1 pathway genes (*29*) were found between the two cell lines
274 to explain the revealed differential dependence and signaling activity (Fig 3D). We noted two
275 missense mutations in the coding regions of *Pik3ca* (p.A423S) and *Rictor* (p.R576S) in 4T07 cells
276 (Fig. 3D; Table S6). Both mutations are in conserved residues and predicted to be of moderate
277 impact (see Supplementary Methods). However, neither have been found in human tumors (n=
278 75,661 patients; see Supplementary Methods), arguing against potential functional relevance.

279 Differential copy number alterations were identified in *Pten*, *Inpp4b*, *Mtor*, *Prr5*, *Tsc1*, and *Akt1s1*
280 (Fig. 3D). Only alterations in *Inpp4b, Tsc1,* and *Akt1s1* correlated with mRNA expression levels
281 between the two lines (Tables S7-S8). Unexpectedly, 4T1 cell DNA demonstrated gain in and
282 mRNA overexpression of *Inpp4b,* a tumor suppressor and a negative regulator of PI3K activity
283 that is frequently lost in basal/triple negative breast cancer (*30, 31*) (Fig 3D; Table S8). On the
284 other hand, 4T1 cells had loss in *Tsc1* and *Akt1s1,* in line with predicting these genes as
285 proliferation suppressors for the 4T1 cells by our CRISPR screens (Fig. 1D). Although these
286 results suggest that 4T1 cells are wired to restrict the negative regulators of the canonical Pi3k
287 pathway, none of these could explain how mTORC1 activity is elevated in 4T07 cells.

288

289 mTORC1 is regulated by the availability of both growth factors and amino acids that feed into
290 independent signaling circuits to collectively tune mTORC1 activity (*26*). Growth factors act
291 through PIK3CA-AKT (*26*), meanwhile amino acids act through different key factors including
292 PIK3C3 (*32*). Accordingly, we investigated mTORC1 activity under different nutritional
293 conditions with the goal of being guided towards the key mTORC1 regulatory mechanisms in
294 4T07 cells. In comparison to 4T1 cells, 4T07 cells maintained higher basal and residual mTORC1
295 activity under serum-fed and starvation conditions, respectively (Fig. 3E). Only amino acid
296 starvation, following overnight serum starvation, abrogated the sustained mTORC1 activity in
297 4T07 cells (Fig. 3E), while amino acid refeeding in serum-free conditions restored the activity
298 back to basal levels (Fig. 3E). Similarly, amino acid refeeding induced the mTORC1 activity in
299 4T1 cells. Collectively, these observations support that mTORC1 is regulated differentially in the
300 two cell lines and pointed out potential significance of the amino acid signaling axis in 4T07 cells.

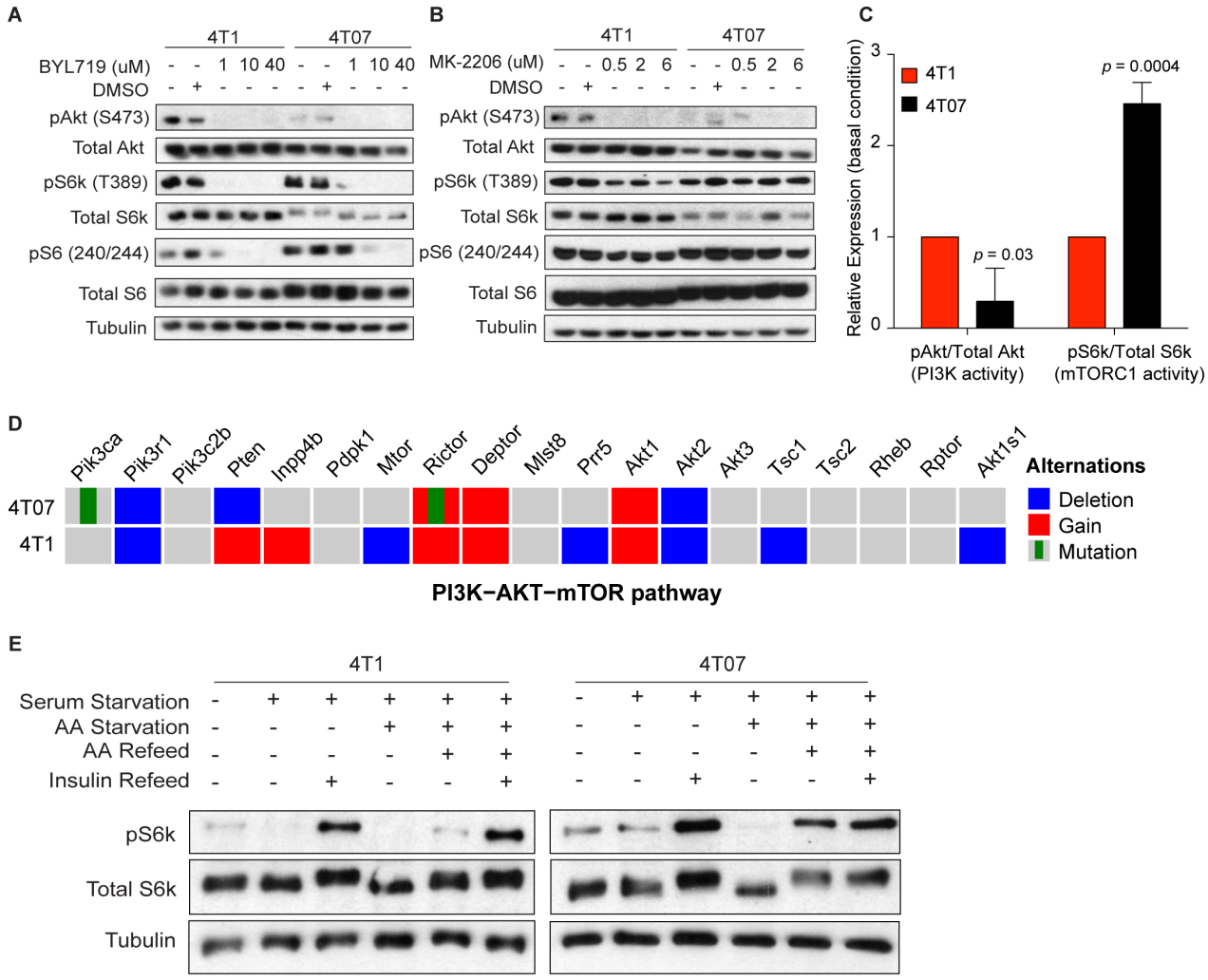

Figure 3

Figure 3. **mTORC1 is differentially regulated in the 4T1 vs. 4T07 cells with higher activity in the 4T07 cells**. **(A-B)** Western blot analysis for the Pi3k-Akt-mTORC1 pathway readouts in the 4T1-4T07 cells upon treating with BYL719 **(A)** or MK-2206 **(B)**. **(C)** Quantification of the relative PI3K and mTORC1 activity in the two cell lines from the performed western blots in (A) and (B). **(D)** Oncoprints for somatic alterations in genes involved in the Pi3k-Akt-mtor pathway in 4T1 and 4T07 cells. **(E)** Western blot analysis assessing mTORC1 activity in the 4T1-4T07 cells under different nutritional conditions. AA; amino acids.

309 **Differential mTORC1 activity is reflected by disparity in lysosomal positioning in 4T1 vs.**
310 **4T07 cells**

311

312 Amino acids stimulate the tethering of mTOR on the lysosomal surface allowing consequent
313 activation (*26*). Furthermore, amino acids activate PIK3C3 to mediate mTORC1 activity (*32, 33*)
314 through different mechanisms such as mediating the peripheral positioning of the lysosomes where
315 mTORC1 demonstrates high activity (*34*), in contrast to when the lysosomes localize at the
316 perinuclear region (*35*). This prompted us to explore the levels of lysosomal mTORC1 in addition
317 to lysosomal positioning in 4T1 and 4T07 cells.

318

319 We assessed the co-localization of Rptor (mTORC1-core component) and the S2448
320 phosphoresidue of the mTOR kinase (more specific to the Rptor-based mTORC1 than the Rictor-
321 based mTORC2 (*36*)), with the lysosomal marker Lamp1 (Fig 4A-B). We observed a diffuse
322 staining pattern for pMtor with a portion being co-localized with Lamp1-positive lysosomes in the
323 two cell lines under basal conditions (Fig 4A-B, 1st row). The level of lysosomal mTORC1 was
324 responsive to nutrient availability. Upon amino acid starvation, mTORC1 localized to small
325 diffuse cytoplasmic puncta (Fig. 4A-B, 2nd row), as previously reported (*37*). Furthermore, this
326 starvation decreased the lysosomal mTORC1 pool in both cell lines (Fig. 4A-C), which was
327 rescued back to basal levels by amino acid refeeding (Fig. 4A-C, 3rd row). We also observed the
328 existence of Rptor in both the cytoplasm, where it co-localizes with Lamp1, and the nucleus (Fig.
329 4A-B). However, the intact mTORC1 appears localized in the cytoplasm in both 4T1 and 4T07
330 cells based on the absence of a pMtor signal from the nucleus, in line with previous studies in
331 different cell types (*38, 39*). We found that 4T07 cells demonstrate a 1.4-fold higher level of
332 lysosomal mTORC1 than 4T1 cells under basal fed conditions (Fig. 4C). We also observed a
333 notable differential lysosomal positioning between the two cell lines. In 4T07 cells, Lamp1-
334 positive lysosomes accumulate at the very tip of cell extensions while in 4T1 they accumulate in
335 the perinuclear region (Fig. 4A-B and 4D; Fig. S5E-G). Interestingly, this peripheral positioning
336 did not change in 4T07 cells by manipulating the nutritional conditions that affected the mTORC1
337 lysosomal co-localization (Fig. 4D). Altogether, these results suggest that lysosomes in 4T07 cells
338 are preferentially positioned at the cellular periphery in comparison to 4T1 cells. Such differences
339 provide mechanistic insights into the differential mTORC1 activity observed between the two
340 lines.

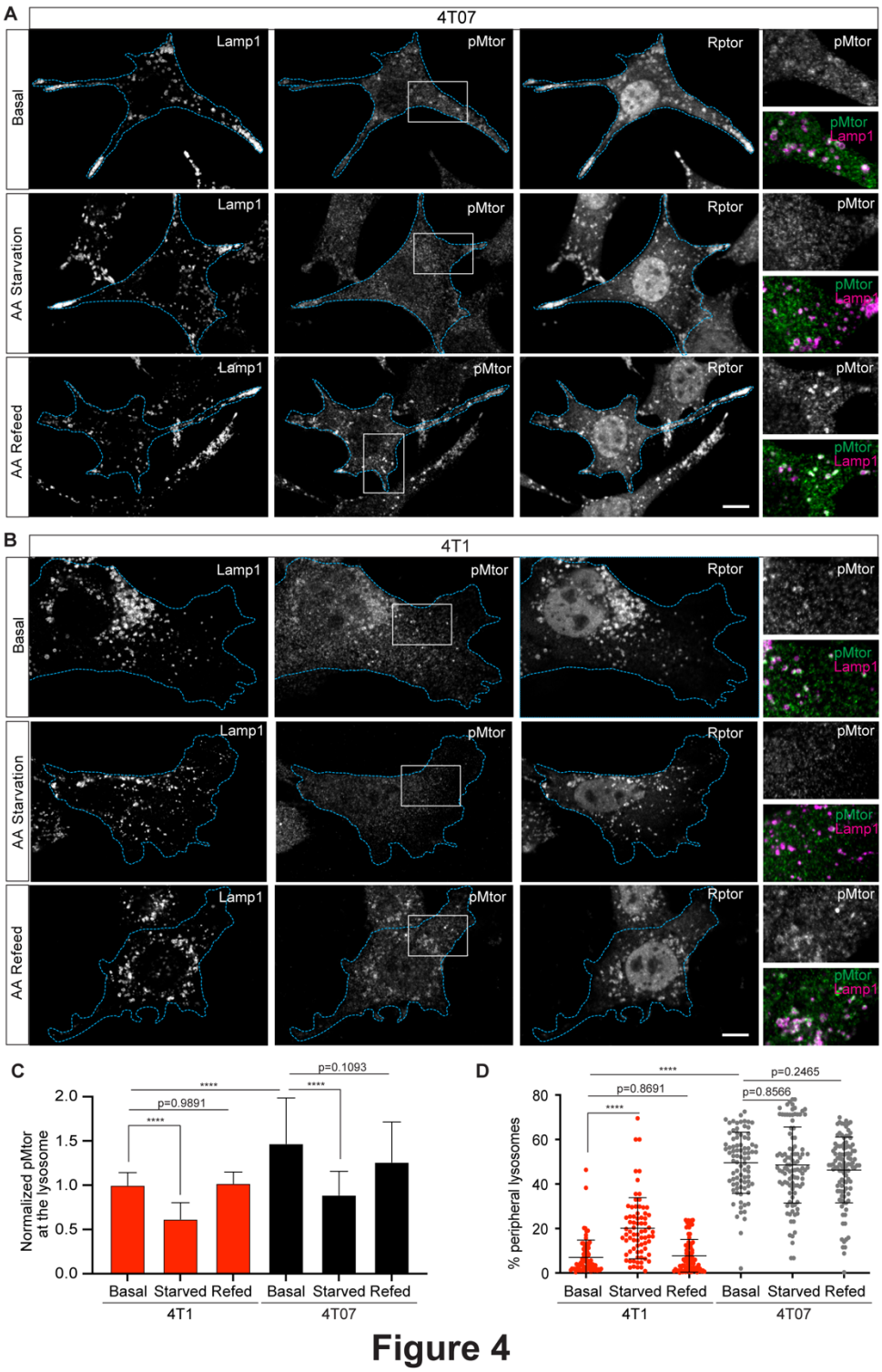

Figure 4

Figure 4. Differential lysosomal positioning between the 4T1 and 4T07 cells. **(A-B)** Immunostaining for the lysosomal marker, Lamp1, and mTORC1 markers, Rptor and pMtor (S2448) in the 4T1-4T07 cells under basal culture conditions or amino acid starvation or amino acid refeeding. **(C)** Quantifications of the mean fluorescence intensity (MFI) of mTORC1 (pMtor signal) on the lysosomes in the two cell lines under the 3 different conditions. **(D)** Graph representing the peripheral lysosomes' percentage in the two cell lines under the 3 different conditions.

349 **PIK3C3 mediates peripheral lysosomal positioning and mTORC1 activity in murine and**
350 **human breast cancer**

351

352 We tested whether inhibiting the Pik3c3 catalytic activity would affect mTORC1 activity and/or
353 lysosomal positioning in the 4T1-4T07 models. Treating 4T07 cells with 1 uM of the VPS34IN1
354 (the selective PIK3C3 inhibitor) for two hours led to 50% decrease in mTORC1 activity (Fig. 5A-
355 B). Parallel treatments of 4T1 cells showed a similar trend, but with higher variability between
356 different replicates given the low basal level of mTORC1 activity in these cells (Fig. 5A-B).
357 Importantly, VPS34IN1 abrogated the response of 4T07 cells to amino acid refeeding after
358 starvation (Fig. S6A), in line with the physiological functions of Pik3c3 (*32-34*). To test whether
359 Pik3c3 regulates lysosomal positioning, 4T07 and 4T1 cells were treated under the same
360 conditions (1 uM of VPS34IN1 for two hours) and then assessed for Lamp1 and pMtor
361 localization. VPS34IN1 mediated a robust 10-fold shift of lysosomes from the periphery to the
362 perinuclear area in 4T07 cells without affecting the tethering of mTORC1 to the lysosomes (Fig.
363 5C-D). Despite the low percentage of peripheral lysosomes in 4T1 cells under basal conditions,
364 VPS34IN1 treatment further reduced it by ~3 fold in comparison to the DMSO-treated control
365 condition (Fig. 5C-D). These results demonstrate that Pik3c3 mediates mTORC1 activity and
366 lysosomal positioning in both cell lines but with differential magnitude given differential basal
367 mTORC1 activity.

368

369 Next, we assessed whether the VPS34IN1-mediated mTORC1 activity suppression would
370 sensitize 4T07 cells to BYL719 treatments. 4T07 cells were treated either with BYL719 alone or
371 combined with 2 uM of VPS34IN1 and their proliferation was assessed for 72 hours. This
372 combination led 4T07 cells to respond to BYL719 as demonstrated by a small, but significant,
373 decrease in their proliferation rate under high doses of BYL719 (30% decrease at 40 uM) (Fig.
374 S6B). We asked whether VPS34IN1 could sensitize 4T07 cells to Pik3ca inhibition that failed to
375 completely abrogate the mTORC1 activity under serum starvation and insulin refeeding, as shown
376 in Fig. S5A-C. Treating serum-starved 4T07 cells with 1 uM of each BYL719 and VPS34IN1 led
377 to a more significant decrease in mTORC1 activity in contrast to single drug treatments that barely
378 affected its activity (Fig. S6C-D). However, VPS34IN1 did not enhance the BYL719 inhibition of
379 mTORC1 activity after stimulating 4T07 cells with insulin (Fig. S6C-D), suggesting that Pik3c3
380 mediates mTORC1 activity mainly via amino acid signalling (*32*).

381

382 We questioned whether the differential dependence and activity of Pik3c3 between the 4T1 and
383 4T07 can be attributed to specific genomic/genetic events. We mined the WGS data for the
384 genomic status of the 3 PI3K classes. Besides carrying the Pik3ca p.A423S missense mutation,
385 the 4T07 cells harbored a Pik3c3 missense mutation in a conserved residue (p.E562K) (Fig. S7A).
386 This residue lies in a loop region of the PIK3C3 kinase domain (Fig. S7B-C) and is found to be
387 mutated in 2 patients (E562A in malignant peripheral nerve sheath tumor, and E562K in penile
388 carcinoma; total n= 75,661 patients) (see Supplementary Methods). However, these mutations are
389 currently of unknown oncogenic potential. In our analysis, the E562K mutation is predicted to be
390 of moderate effect (Table S6). To investigate whether this mutation mediates higher activity of
391 PIK3C3 and hence higher mTORC1 activity, we generated HeLa Flp-In T-REx cells that express
392 either wildtype or mutated PIK3C3 in a tetracycline inducible manner. Inducing the expression of
393 the two forms of the PIK3C3 protein did not lead to a significant difference in mTORC1 activity
394 (Fig. S7D). It is therefore unlikely that this mutation underlies the mTORC1 hyperactivity in 4T07
395 cells. Overall, we did not pinpoint any other notable differences between the two lines that can
396 explain the revealed molecular and biological phenotypes (Fig. S7A). For instance, despite the

397 identified *Pik3c3* genomic deletion in 4T1 cells, there is no significant difference in the *Pik3c3*
398 mRNA levels between the two lines (Table S8).

399

400 Next, we examined whether the observations we made in the 4T1-4T07 murine cells are present
401 in human breast cancer. For this, we interrogated early passages of breast cancer patient-derived
402 xenograft (PDX) derived cell lines (*40*) for mTORC1 activity (Fig. S8A-B). This identified 2
403 potential PDX cell lines (1915 and 1735) with high mTORC1 activity. We chose to focus on the
404 PDX line 1915 since it originated from a patient with basal breast cancer (*40*), the same intrinsic
405 subtype that the 4T1-4T07 cells recapitulated. In addition, the patient from which PDX 1915 was
406 derived was diagnosed with a metastatic relapse 1.5 years after the surgical resection of the primary
407 tumor, hence recapitulating the clinical problem of metastatic latency (Fig. S8C). The WGS of the
408 patient tumor and the generated PDX suggested that the patient was free from *PIK3CA* activating
409 hotspot mutations or a *PTEN* deletion (like 4T1-4T07 cells) which frequently underlies mTORC1
410 hyperactivity (Fig. S8C). PDX1915 harbored an amplification in the *PIK3CA* gene, without
411 observed overexpression in its transcript in comparison with PDXs harboring a WT non-amplified
412 or altered *PIK3CA* gene (Fig. S8D). We explored whether inhibiting PIK3C3 activity would
413 dampen mTORC1 activity in PDX 1915 cells and found that VPS34IN1 decreased mTORC1
414 activity approximately 50% by western blot analysis (Fig. 5E-F). We asked whether this effect is
415 paralleled with a shift in the lysosomal positioning towards the perinuclear region. VPS34IN1
416 significantly reduced the percentage of peripheral lysosomes (Fig. 5G-H). Notably, PDX 1915
417 cells under basal conditions showed a high level of heterogeneity in terms of the lysosomal
418 position (Fig. 5G-H), hence recapitulating the characteristic heterogeneity of human tumors. Also,
419 we noticed a significant increase in the percentage of cells with tubulated lysosomes in the
420 VPS34IN1-treated condition (Fig. 5G and 5I), consistent with a previous report (*41*).

421

422 Altogether, these data support that inhibiting PIK3C3 activity in breast cancer cells leads to a
423 perinuclear positioning of the lysosomes, hence reducing mTORC1 activity. However, this
424 signaling circuit appears more profound in cells with preferential peripheral lysosomal positioning.

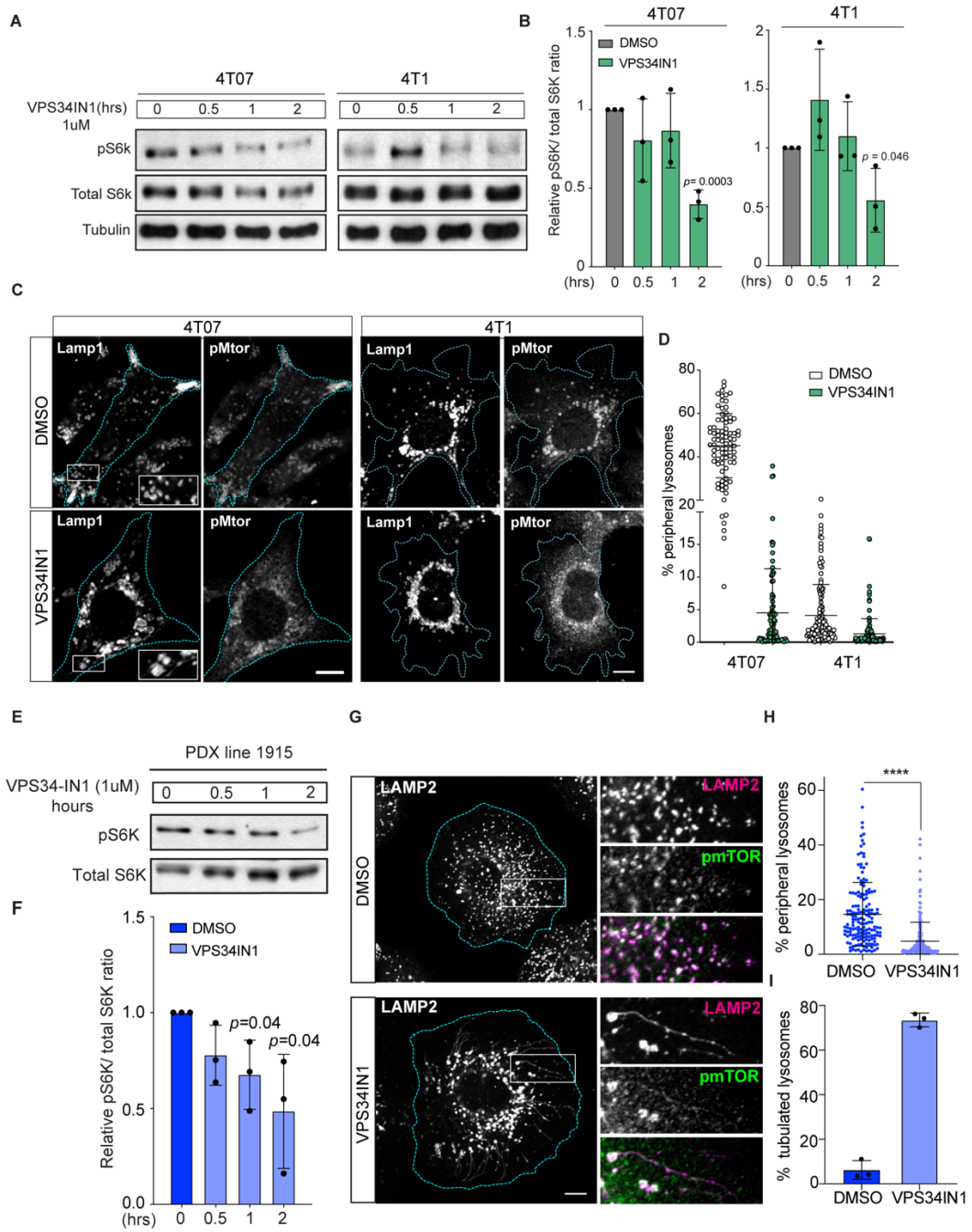

Figure 5

Figure 5. **PIK3C3 mediates peripheral lysosomal positioning and mTORC1 activity in murine and human breast cancer. (A)** Western blot analysis for the VPS34IN1 effect on 4T07 and 4T1 cells' mTORC1 activity. **(B)** Quantification for mTORC1 activity in panel (A). **(C)** Immunostaining for Lamp1 and pMtor in 4T07 and 4T1 cells under the effect of VPS34IN1 (2 hours). **(D)** Quantifications of the percentage of peripheral lysosomes in the VPS34IN1-treated cells in comparison to the control condition (DMSO-treated). **(E)** Western blot analysis for the VPS34IN1 effect on mTORC1 activity in the PDX-1915. **(F)** Quantification for the mTORC1 activity in panel (E). **(G)** Immunostaining for LAMP2 and pmTOR in the PDX-1915 cells under the effect of VPS34IN1 (2 uM) or DMSO (for 2 hours). **(H)** Quantifications of the percentage of peripheral lysosomes in (G). **(I)** Quantifications of the percentage of tubulated lysosomes in (G).

437 **High mTORC1 activity in primary tumors correlates with worse clinical outcome in breast**
438 **cancer patients**

439

440 We next asked whether mTORC1 activity can predict relapse incidence and/or worse clinical
441 outcome in breast cancer patients. The high expression of RPS6KB1, encoding the canonical
442 mTORC1 effector S6K1, correlates with worse distant metastasis-free survival in patients with
443 early breast cancer (*42*). Since the expression level does not necessarily correspond to high
444 mTORC1 activity, we sought to complement this notion by investigating mTOR signaling-
445 associated gene signatures as a surrogate for the pathway activity. Using a single-sample Gene Set
446 Enrichment Analysis (ssGSEA), we generated an "mTORC1 score" for each patient's tumor in
447 the METABRIC and TCGA-BRCA cohorts based on a previously annotated and well-curated
448 mTORC1 signaling-mediated signature (*43*) (Fig. 6A). We observed that Basal and HER2 positive
449 breast tumors tend to show a higher mTORC1 activity signature in comparison with the less
450 aggressive luminal subtypes (*2*) (Fig. 6B). We also found that patients bearing tumors with high
451 mTORC1 signature score tend to have worse prognosis in comparison to those with low scores in
452 the METABRIC dataset ($p<0.0001$) with a trend towards a similar correlation in the TCGA dataset
453 ($p=0.06$) (Fig. 6C). These results align with the established impact of mTORC1 activity in human
454 cancer (*44*) and rationalize exploring novel therapeutic strategies to target this activity in breast
455 cancer. Therefore, we wondered whether the therapeutic targeting of the revealed PIK3C3-
456 mTORC1 circuit in animal models would have a beneficial outcome on breast cancer progression
457 and metastasis burden.
458

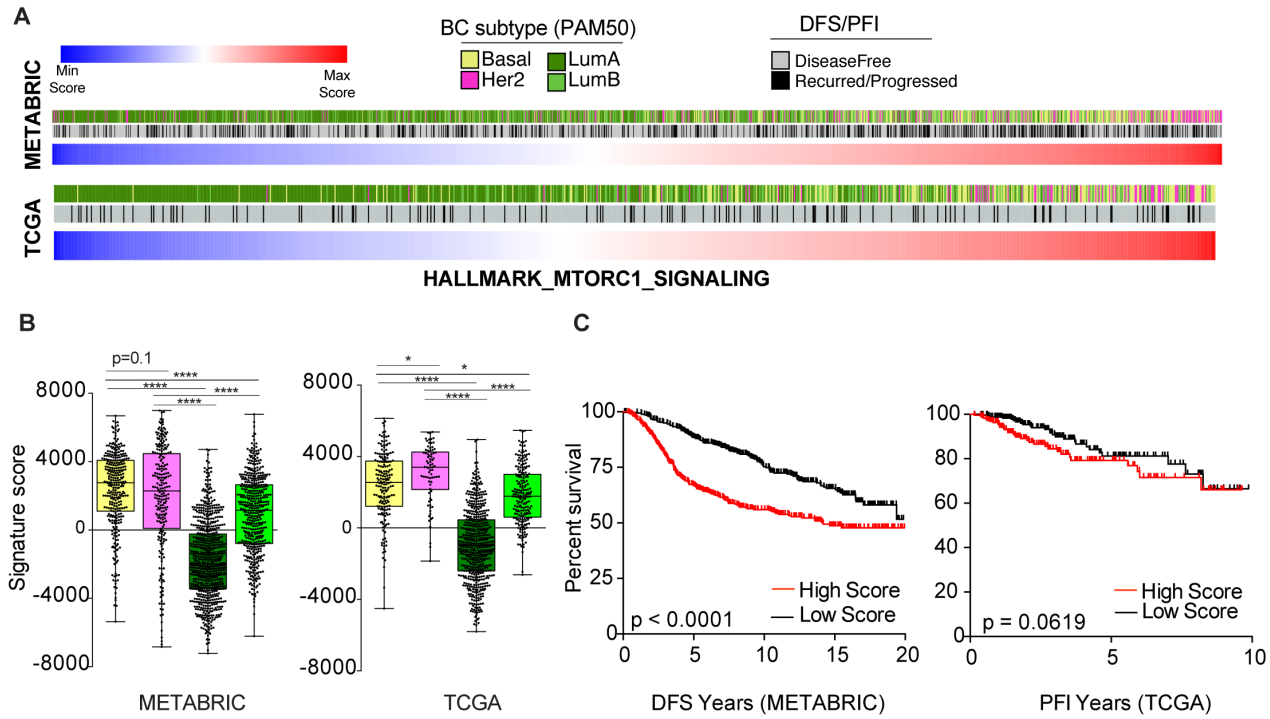

Figure 6

Figure 6. High mTORC1 activity correlates with worse outcome in breast cancer patients. **(A)** Heatmaps showing ssGSEA ranked by the Hallmark_mTORC1_Signaling signature score. Breast cancer samples were stratified according to their intrinsic molecular subtype based on gene expression profiling. **(B)** Comparing different breast cancer subtypes according to the Hallmark_mTORC1_Signaling signature score in the METABRIC and TCGA datasets. **(C)** Kaplan–Meier curves of disease-free survival and progression-free interval from the METABRIC and TCGA datasets, respectively.

469 **Inhibiting Pik3c3 decreases *in vivo* metastatic burden specifically in the 4T07 model**

470

471 We performed spontaneous metastasis assays using the 4T07 and 4T1 models in the presence or
472 absence of VPS34IN1. We implanted 4T07 cells expressing GFP and luciferase (hereafter 4T07-
473 TGL (*12*)) in the mammary fat pad of nude mice to bypass the technical challenge of the immune
474 system-mediated elimination of GFP-positive cells in an immunocompetent context (*45*) (Fig. 7A).
475 One week after implanting cells, mice were randomized to receive either the vehicle or VPS34IN1
476 (50 mg/kg/day) (Fig. 7A). Six days after starting treatment, half of the mice were sacrificed for an
477 early timepoint analysis (Fig 7A). Tumor weight did not differ between the two groups, suggesting
478 no effect on the primary tumor burden (Fig. 7B). We then analyzed the burden of disseminated
479 tumor cells (DTCs) by dissecting the lungs and quantifying the metastatic burden by
480 bioluminescence imaging (BLI). The VPS34IN1-treated mice had significantly lower DTC burden
481 than the control group (Fig. 7C-D). Next, we analyzed the second group of mice after 12 days of
482 treatment by either the VPS34IN1 or the vehicle (3 weeks post implantation). No statistically
483 different change in tumor weight between the two experimental groups was observed (Fig. 7B).
484 However, the incidence of visible metastases in the treated group (1/5 mice) was 40% of that of
485 the control group (3/6 mice) (Fig. 7E). Analyzing the digested lungs of mice that showed no visible
486 lung metastases suggested that the VPS34IN1-treated mice demonstrated a trend towards lower
487 DTC burden in comparison to the control group (p=0.06) (Fig. S9A). Next, we asked whether
488 VPS34IN1 affected mTORC1 activity *in vivo*. Indeed, lower mTORC1 activity in the VPS34IN1-
489 treated mice versus the control group was observed (Fig. S9B-C). Altogether, these data suggest
490 that pharmacological targeting of the Pik3c3-mTORC1 signaling axis decreases the DTC burden,
491 hence minimizing the incidence of metastasis.

492

493 To compare 4T07 and 4T1 models, we implanted 4T1-TGL cells in the mammary fat pad of nude
494 mice (Fig. 7F). One week later, we started the treatment with either VPS34IN1 (50 mg/kg/day) or
495 vehicle for two weeks before analyzing the primary tumor and metastasis burden. We did not
496 observe significant differences between the two groups with respect to primary tumor burden (Fig.
497 7G), or incidence of metastasis (Fig. 7H), despite the trend towards a reduction in mTORC1
498 activity in the 4T1 primary tumors (Fig. S9D-E). Notably, the metastasis burden was higher in the
499 4T1-tumor bearing mice in comparison to 4T07-tumor bearing mice (see the BLI scale in Fig. 7E
500 and 7H). This reinforces the proposal that 4T1 is a more aggressive subclone with higher ability
501 of fulfilling the metastatic cascade than the 4T07, even in conditions permitting the latter to
502 generate overt metastases (*10*).

503

504 To exclude the possibility that saturated BLI signals emitted by the 4T1 overt metastases precluded
505 or masked the effect of VPS34IN1 on less developed lesions (i.e., micrometastases), we undertook
506 a complementary approach in syngeneic mice. We implanted the parental 4T1 cells in the
507 mammary fat pad of immunocompetent BALB/c mice and after two weeks, the generated primary
508 tumors were surgically resected (Fig. 7I). After letting the mice recover from the surgical
509 procedure, they were randomized either to receive VPS34IN1 (50 mg/kg/day) or vehicle for a
510 week before analyzing the burden of lung metastasis by immunohistochemistry. Like the prior
511 experiments, there was no difference in the incidence of metastasis since the two experimental
512 groups demonstrated a 100% incidence rate (Fig. 7J). Moreover, there was no significant
513 difference in the burden of metastasis with respect to the number or size of metastatic lesions (Fig.
514 7K-M). Collectively, these results demonstrate that pharmacological targeting of the revealed
515 Pik3c3-mTORC1 circuit blunts breast cancer metastasis, preferentially in models with peripheral
516 lysosomal positioning and high mTORC1 activity.

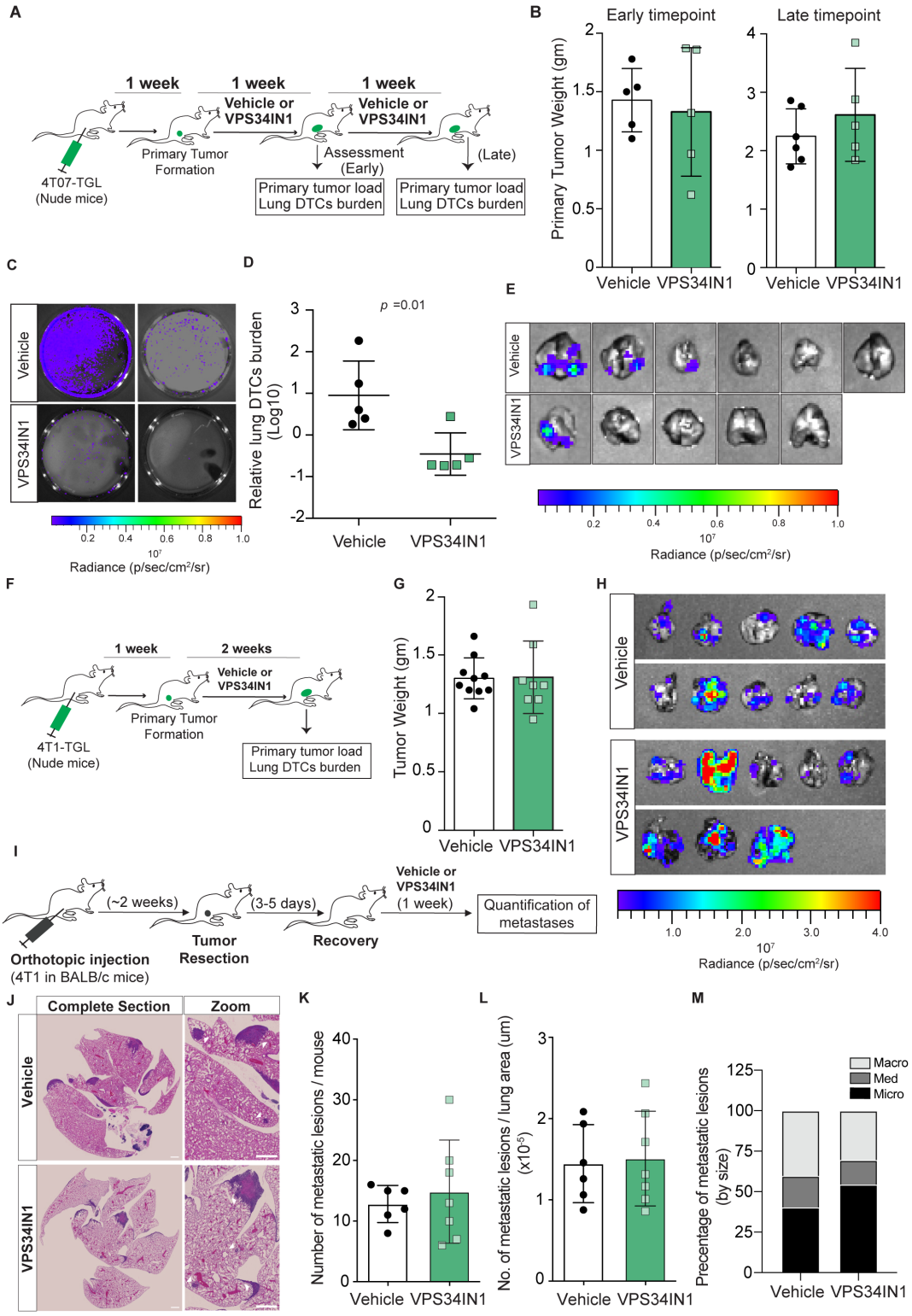

Figure 7

Figure 7. Inhibiting the Pik3c3-mTORC1 axis decreases the metastatic burden in vivo preferentially in the 4T07 model. **(A)** Schematic of the experiment investigating the effect of Pik3c3 inhibition on the metastasis burden in the 4T07 model. **(B)** Graph showing tumor weight of mice treated with either VPS34IN1 or vehicle at the early and late experimental endpoints. **(C)** Representative images of the lung DTCs burden in 4T07-bearing mice treated with VPS34IN1 or vehicle at the early experimental endpoint (n=5/group). **(D)** Quantification of relative lung DTCs burden between the two groups in (C). **(E)** Representative ex-vivo lung images of 4T07-bearing

525 mice treated with VPS34IN1 or vehicle at the experimental late endpoint. **(F)** Schematic of the
526 experiment investigating the effect of Pik3c3 inhibition on the metastasis burden in 4T1 tumors-
527 bearing nude mice. **(G)** Graph showing tumor weight of mice treated with either VPS34IN1 or
528 vehicle at the experimental endpoint. **(H)** Representative ex-vivo lung images of 4T1 tumors-
529 bearing mice treated with VPS34IN1 or vehicle at the experimental endpoint. **(I)** Schematic of the
530 experiment investigating the effect of Pik3c3 inhibition on the metastasis burden in 4T1 tumors-
531 bearing BALB/c mice. **(J)** Representative H&E stainings of lungs obtained from mice in (I). **(K-**
532 **M)** Quantifications of the metastasis burden: absolute number of lesions **(K)**, number of lesions
533 normalized to lung area **(L)**, and percentage of different sizes of metastases **(M)** in the vehicle-
534 and VPS34IN1-treated mice.

535 **DISCUSSION**

536

537 The landscape of the differential cancer cell-specific intrinsic factors contributing to their
538 metastatic fate and response to therapies remains poorly outlined. Here, by comparing two related
539 basal B like breast cancer models, 4T1 and 4T07 that display differential metastatic and dormancy
540 capacity, as well as primary cells derived from basal breast cancer patient derived xenograft, we
541 show that metastatic cells depend on high PI3K activity in comparison with dormancy-prone cells.
542 These observations complement early reports demonstrating that bone marrow derived DTCs from
543 breast cancer patients during the metastatic latency period had low PI3K activity (*28, 46*). Despite
544 the observed lower PI3K-AKT activity in the dormancy-prone 4T07 cells (this study) and shown
545 previously in D-HEp3 cells (a model of dormant human head and neck carcinoma (*28*)), these two
546 cell lines showed higher mTORC1 activity than their metastatic counterparts, 4T1 and T-HEp3
547 (also shown previously (*28*)), respectively.

548

549 An unexpected finding in our study is that the peripheral lysosomal positioning contributes to high
550 mTORC1 activity in the dormancy-prone cells despite low PI3K activity. Previous studies (*34,*
551 *35*) have established that peripheral localization of the lysosomes mediates mTORC1 activation,
552 while perinuclear clustering dampens this activity and accordingly enhances the macroautophagic
553 dynamics (*35*). Our results suggest that the 4T1-4T07 cell line pair potentially follows this binary
554 model. Whether this is also reflected in a differential autophagic potential between the two lines
555 would be worth exploring in future studies given the contradictory reports regarding the role of
556 autophagy in regulating dormancy (*47, 48*).

557

558 Class-III PI3K, PIK3C3, activates mTORC1(*32*) through different mechanisms (*24, 27, 34, 49*),
559 such as inducing the anterograde transport of the lysosomes to the cell periphery, where mTORC1
560 gets activated (*34*). Here, we found that inhibiting Pik3c3 activity reversed the constant peripheral
561 lysosomal positioning and the ensuing high mTORC1 activity in dormancy-prone cells. This
562 inhibition further limited the ability of these cells to colonize lung tissues and to generate overt
563 metastases under permissive conditions, supporting a role for this molecular machinery in
564 achieving successful metastasis. Consistent with a conserved role in human tumors, PIK3C3
565 inhibition mediated a similar molecular action in a line derived from a breast cancer metastatic
566 relapse patient. Notably, there is also the possibility of mTORC1-independent mechanisms
567 underlying the effects of PIK3C3 inhibition or alternative PIK3C3-independent mechanisms
568 contributing to the lysosomal positioning and/or mTORC1 hyperactivity (*50*) in dormancy-prone
569 cells. Extending knowledge in theses directions would guide future exploration of the genetic and
570 signalling dependence of dormancy-prone cells.

571

572 mTORC1 and PIK3C3 have an entangled bilateral relationship. We focused on PIK3C3 acting
573 upstream of mTORC1, but mTORC1 is also reported to act upstream of PIK3C3 to mediate
574 lysosomal regeneration after starvation-induced autophagy to support cell survival (*41, 51*). These
575 studies characterized the tubulated lysosomes as autophagy-induced transient structures that serve
576 as proto-lysosomes during the lysosomes' regeneration (*51*). However, these structures were also
577 found under basal nutrient-rich conditions (*41*). In both cases, their formation was dependent on
578 mTORC1 activity. Here, in the PDX1915 primary cell line, under basal nutrient-rich conditions,
579 we observed that existence of these structures was further augmented upon treatment with
580 VPS34IN1, despite the reduction in mTORC1 activity. Whether this increased tubulation is a
581 feedback mechanism induced by the mTORC1 activity reduction to secure a sufficient lysosomal

582 pool for mTORC1 activation is unclear. The potential connection between the lysosomal
583 positioning, mTORC1 activity, autophagy, and the ability to form tubules should be further
584 investigated.

585

586 From a therapeutic perspective, Gedatolisib, a dual Class-I PI3K/mTOR inhibitor, as a single agent
587 or combined with standard-of-care chemotherapy, failed to impact the metastatic burden in two
588 breast cancer models (*52*). Another study demonstrated that long term pharmacological inhibition
589 of PI3K or AKT induces a PIK3C3-SGK3 signaling axis to activate mTORC1 and that targeting
590 this axis can revert the induced resistance towards the PI3K-AKT inhibition (*27*). Our work
591 demonstrating that dormancy-prone cells do not depend on the class-I PI3K and are resistant to its
592 pharmacological inhibition meanwhile being dependent on the class-III PI3K complements these
593 studies. Whether the combinatory inhibition of class-I and -III PI3K, and mTORC1 would be an
594 effective method to minimize the metastatic burden in vivo should be explored in future studies.

595

596 While our CRISPR screening approach revealed novel insights into the intrinsic differences
597 between cells of differential metastatic capacity, it has limitations. The screens were performed,
598 for technical feasibility, in an *in vitro* setting that does not necessarily recapitulate the impact of
599 the crosstalk with microenvironment on gene essentiality and signaling pathways' activity.
600 Nonetheless, we extensively validated the PI3K(s)-mTORC1 signaling circuits in vitro and in
601 vivo. Another limitation of our study is depending on one pair of cell lines with validations in a
602 patient-derived xenograft. Whether these findings could be extended in other models would be
603 worth addressing in future studies. Such a limitation goes back-to-back with the global challenge
604 of scarce authentic cell line pairs that possess different metastatic potentials upon being implanted
605 in syngeneic mice (*8*).

606

607 In summary, the work described here provides novel insights into the intrinsic differences between
608 cells of differential metastatic capacity that can guide future explorations of the biology and
609 therapeutic vulnerabilities of breast cancer metastatic relapses.
610

611 **Materials and Methods**

612

613 **Cell lines, PDX lines, and reagents**

614

615 Parental 4T07 cells (*9*) were obtained from the Karmanos Cancer Institute, Wayne State
616 University. The 4T07-TGL cells (*12*) (Memorial Sloan Kettering Cancer Center, MSKCC) were
617 obtained from Dr. Filippo Giancotti (Herbert Irving Comprehensive Cancer Center, HICCC). 4T1
618 cells were obtained from ATCC. To generate 4T1-TGL cells, HEK293T cells were seeded in 6 cm
619 plates and transfected with 3 ug of TGL vector (*53*) (gift from Dr. Vladimir Ponomarev, MSKCC)
620 and 3 ug of pCL-Ampho using $CaCl_2$ towards retroviral production. Then parental 4T1 cells were
621 infected and stable 4T1-TGL cells were generated and established after sorting for GFP positive
622 cells. All the 4T1 and 4T07 cell lines were cultured in Dulbecco's modified Eagle's medium
623 (DMEM; Wisent #319-005-CL), supplemented with 10% fetal bovine serum (FBS; Gibco), and
624 1% penicillin/streptomycin (P/S) antibiotics (Wisent).

625

626 For serum starvation, cells were cultured overnight (O/N) in serum-free DMEM supplemented
627 with 1% P/S. For amino acids starvation, cells were first serum starved O/N, then rinsed with PBS
628 and incubated in Earle's Balanced Salt Solution (EBSS; ThermoFisher Scientific #24010043)) for
629 two hours at 37 °C. Refeeding with serum was done by replacing the serum-free DMEM with 10%
630 FBS-supplied DMEM. To refeed with insulin, 100 nM insulin (Humulin R U-100) was added to
631 the serum-free DMEM, and cells were incubated for 30 minutes at 37 °C. To refeed with amino
632 acids, MEM Amino Acids solution (50x; Sigma-Aldrich M5550) was added to the EBSS (1:50),
633 and cells were incubated for 30 minutes at 37 °C.

634

635 All Patient-derived xenograft (PDX) epithelial cell lines were derived from tissues obtained
636 according to the ethical regulations of McGill University and after informed consents, as stated
637 previously (*40*). PDX 1915 (*40*) was cultured in DMEM (Gibco - 11995-065) and F-12 Nutrient
638 Mixture (Ham) (Gibco-11765-054) (1:4), 5% FBS (Life Technologies, #12483012), 0.4 ug/mL
639 Hydrocortisone (Sigma-Aldrich #H0888-1G), 5 ug/mL Insulin (Gibco-12585-014), 8.4 ng/mL
640 Cholera toxin (Sigma-Aldrich #C8052), 10 ng/mL Epidermal growth factor (BPS bioscience
641 #90201-1), 10 umol/L Y-27632 (Abmole #M1817), 50 ug/mL Gentamicin (Gibco - 15710-072),
642 1% P/S (Thermo Fisher Scientific, #15140-122), Amphotericin B (1 ug/ml) (Thermo Fisher
643 Scientific, #15290026).

644

645 The PIK3CA-inhibitor BYL719 (ChemieTek), AKT-inhibitor MK-2206 2HCl (Selleck Chemicals
646 #S1078), and VPS34-IN1 (Cayman Chemical #17392) were dissolved in DMSO and used in
647 different concentrations as indicated.

648

649 **CRISPR-Cas9 Screening**

650

651 The mouse Genome-Scale CRISPR Knock-Out (mGeCKO) library A (Addgene #1000000052),
652 composed of ~68,000 gRNAs: 3 gRNAs/gene, 4 gRNAs/miRNA, and 1000 nontargeting
653 sequence, was amplified and prepared for NGS (MiSeq Illumina) to assess the gRNA distribution
654 and library quality, as previously described (*20*). In reference to the original library, the assessed
655 parameters of the amplified library (percentage of undetected gRNAs and perfectly matching

656 gRNAs in addition to the skew ratio of the top 10% represented gRNAs to bottom 10%) were all
657 within the recommended ranges for a reliable library (*20*).

658

659 Lentiviral production was performed as previously described (*20*). Briefly, low passage HEK
660 293FT cells were plated in Nunc EasYFlask cell culture flasks (Thermo Fisher Scientific) and
661 transfected, using lipofectamine 2000 (Thermo Fisher Scientific), with psPAX2 (23.4 µg),
662 pMD2.G (15.3 µg), and 30.6 µg of the lentiCRISPR V2 vector encompassing the Cas9 in addition
663 to the amplified library. 48 hours later, the viruses-containing media was collected and filtered
664 using 0.45 um sterile filters (Sarstedt #83.1826). A multiplicity of infection (MOI) test was
665 performed to define the optimum volume of the viruses-containing media to be used for the
666 screens.

667

668 The 4T1 and 4T07 cells were infected independently, as previously described (*20*). Briefly, the
669 two cell lines were seeded in 12 well plates (1.5-2 x 10^6 cells/well) and then subjected to
670 spinfection (MOI < 0.3) by centrifugation at 2,000 RPM for 2 hours at 33°C in the presence of
671 polybrene (10 ug/ml). This method allowed ~1300-fold coverage of the mGeCKO library A. After
672 24 hours, cells were trypsinized, pooled, and seeded in 15 cm plates in media containing
673 puromycin for selection (3 ug/ml for the 4T07 cells and 2 ug/ml for the 4T1 cells). Cells were
674 propagated under selection for a week while maintaining a library coverage of at least 700-fold
675 (50 x 10^6 cells). Then, the first time point (T0) was collected (50 x 10^6 cells/timepoint to keep the
676 stated fold coverage). The cells were propagated in a similar manner while collecting the
677 consequent timepoints (T1, T2, T3). The collected cells were spin down in 15 ml tubes and kept
678 in -80 °C until they were processed. Every screen was repeated three independent times following
679 the same procedure, where replicates were annotated A, B, and C (as shown in Fig. S2). The
680 collected samples were then processed for genomic DNA (gDNA) extraction according to the
681 manufacturer's protocol (Zymo Research Quick-gDNA MidiPrep Plus kit, #D4075) and prepared
682 for NGS (HiSeq 4000 Illumina) as previously described (*20*).

683

684 **CRISPR-Cas9 Screen Analysis**

685

686 The count and test commands of MAGeCK (*54*) (Version 0.5.7) were used to generate read counts
687 for each gRNA and to determine the positively selected genes in T3 in reference to T0,
688 respectively. A range of 483-744 and 529-881 fold library coverage for 4T07 and 4T1 screens,
689 respectively was defined by sequencing (recommended 100-300 fold coverage). The BAGEL
690 software (*55, 56*) (v0.91) was then used to calculate the foldchange of gRNA representations in
691 different timepoints in reference to T0. Consequently, using BAGEL, each gene was assigned a
692 Bayes Factor (BF) as a confidence measure of fitness or essentiality. To execute this, BAGEL
693 depends on a pre-set list of essential and non-essential genes (*14, 55, 57*). This analysis was
694 performed for each timepoint individually and using the final 2 timepoints combined as has been
695 previously described (*22*). For downstream analysis, we utilized BF scores from the final 2
696 timepoint analysis. A strict threshold of normalized BF > 6 was used to consider a gene essential
697 in our screens (*57*). As stated in the main text, the generated BF scores were then used for the
698 Precision-Recall analyses based on previously annotated gene lists (essential and non-essential)
699 (results are demonstrated in Fig. S2E-F). To compare the essential genes' profile of the two cell
700 lines, the difference between the BF scores of the two lines was calculated. Then, a Z-score for the
701 difference in BF for each gene was calculated (Table S2-4). Positive Z-score denoted 4T1-specific
702 essential gene and negative Z-score denoted 4T07-specific essential gene.

703 **Immunostaining, confocal microscopy, and image analysis**

704

705 Cells were plated on fibronectin-coated glass coverslips to desired confluence ~6 hrs. For amino
706 acid starvation, cells were serum starved (O/N; for 16 hrs), then incubated with EBSS for 2hrs.
707 For re-feeding, 50x MEM amino acids solution was diluted to 1X into EBSS and added to the cells
708 for 30 minutes. Cells were fixed with 3.7% formaldehyde in CSK buffer (100mM NaCl, 300mM
709 Sucrose, 3mM MgCl2, 10mM Pipes pH 6.8) for 15 min. Immunostaining was performed in
710 saponin buffer (TBS supplemented with 1% BSA, 0.01% saponin) using the following antibodies:
711 Rat anti-LAMP1 (Abcam #ab25245) at a concentration 1/400, Mouse anti-LAMP-2
712 (Developmental Studies Hybridoma Bank #H4B4) at a concentration 1:50, Mouse anti-
713 phospho(Ser2448)-mTOR (Cell Signaling Technology #2971) at a concentration 1:200, and
714 Rabbit anti-Rptor (14C4) (Bioss antibodies, #51285M) at a concentration 1:100. Images were
715 collected from a Zeiss confocal LSM700 (Carl Zeiss, Jena, Germany) microscope with oil
716 immersion objective lenses (Plan-Apochromat, 60×, 1.40 numerical aperture NA; Carl Zeiss).

717

718 Image analysis was performed using the FIJI software version 2.3. For measurement of pmTOR
719 at the lysosomes, a region of interest corresponding to the lysosomes was created using the auto-
720 threshold of the LAMP1 channel and was transferred to the corresponding background subtracted
721 pmTOR channel to measure the mean fluorescence intensity (MFI) at the lysosomes. Data
722 represent the mean with SD of at least 30 images from three independent experiments. Statistical
723 significance was determined using one-way ANOVA test with a confidence interval of 95%. The
724 lysosome distribution was measured from confocal images of LAMP1 and pmTOR co-staining
725 captured as described above. For at least 75 cells per condition, a single line, five pixels in width,
726 was traced manually from the center of the nucleus to the cell edge as delineated by pmTOR
727 staining (See Fig. S5). The intensity values along this line were obtained using the "plot profile"
728 plugin from FIJI. The mean fluorescence intensity and the positions along the line for each cell
729 were normalized from 0 to 1 using Matlab as used in reference (*58*). The normalized data were
730 transferred to Prism 9 software (GraphPad Prism, GraphPad Software, San Diego CA) for further
731 analyses. The percentage of signal at the periphery was calculated by dividing the area under the
732 curve (AUC) between positions 0.75 to 1 by the total AUC between positions 0 to 1. Data are
733 representative of three independent experiments and are shown as the mean with SD (n>75).
734 Statistical significance was determined using the non-parametric Mann-Whitney test with a
735 confidence interval of 95% (****, p-value < 0.0001). This test analysis compares the distributions
736 of two unpaired groups. Data are shown as the mean with SD. For tubulation quantification, the
737 percentage of cells presenting at least one tubulated lysosome was determined among at least 220
738 cells per condition from three independent experiments. The percentages in the DMSO- and
739 VPS34IN1-treated cells (PDX1915) were then compared by a two-tailed t-test to calculate the *p*-
740 value as stated on the figure.

741

742 **Animal Studies**

743

744 All animal experiments were performed in accordance with the Canadian Council of Animal Care
745 guidelines and approved by the Animal Care Committee of the Montreal Clinical Research
746 Institute (IRCM).

747

748 ***Primary tumor and spontaneous metastasis assays.*** 1x10^5 4T07-TGL or 4T1-TGL cells were
749 injected in the fat pad of the 4th mammary gland of 6-week-old NU/J mice (The Jackson laboratory
750 #002019). For the 4T07 experiment, 1-week post-injection, the mice were randomized into two
751 groups to receive either vehicle (5% DMSO in corn oil) or VPS34IN1 (50 mg/kg/day) by oral
752 gavage daily for either 6 days or 12 days. For the 4T1 experiment (in nude mice), 1-week post-
753 injection, mice were randomized to receive either vehicle or VPS34IN1 (50 mg/kg/day) for two
754 weeks.

755

756 For experiments in (Fig. 7J-M), 5x10^5 4T1 cells were injected in the fat pad of the 4th mammary
757 gland of 8–10-week-old BALB/c mice (The Jackson Laboratory #0651). Two weeks later, primary
758 tumors were resected. Mice were left to recover for ~3-5 days, then randomized for treatments
759 with either vehicle or VPS34IN1 for a week as described above. At the experimental endpoint,
760 Mice with recurred primary tumors were excluded from the final analyses presented in Fig. 7.
761 Otherwise, mice were sacrificed, and lungs were collected immediately, emersed in PBS then fixed
762 in 4% PFA for 24 hr at 4ºC. Lungs were then placed in 70% ethanol before being embedded in
763 paraffin. Paraffin blocks were then sectioned at 4 µm thickness and processed for H&E staining
764 and the 20X objective of the Aperio-XT slide scanner (Leica Biosystems) was used to scan slides.
765 Fiji (ImageJ) was used to visualize the generated images and measure size of metastatic lesions.
766 Given the irregularity between different lesions, the length of the longest dimension was
767 considered as a measure to categorize micrometastases (< 100 um), macrometastases (> 200 um)
768 and lesions scoring in between (100-200 um). The vehicle and VPS34IN1-treated groups were
769 compared by a two-tailed t-test to calculate the *p*-value (n= 6 or 7 mice/group).

770

771 ***Lung Disseminated tumor cells (DTCs) burden in 4T07 (early timepoint).*** At the experimental
772 endpoint, mice were euthanized, and lungs were processed as previously described (*6*). Briefly,
773 lungs were dissected and immediately emersed in PBS and cut into small pieces. Then, the lung
774 pieces were digested in PBS supplemented with 75 µg/ml TH Liberase (Roche 05401127001), 75
775 µg/ml TM Liberase (Roche #05401151001), and 12.5 µg/ml DNase. Samples were then incubated
776 in the digestion buffer on a rotor in 37 °C. Samples were then centrifuged at 1,300 RPM for 5
777 minutes and supernatant was discarded. Pellets were resuspended in PBS, pipetted up and down
778 multiple times and filtered through a 70 µm strainer to get rid of the undigested lung pieces. 1 ml
779 of Red Blood Cells Lysis Solution (Sigma, R7757-100ML) was then added to each sample and
780 the manufacturer protocol was followed. Cells were finally seeded in 15 cm plates in Thioguanine-
781 containing DMEM Wisent media supplied with 10% FBS and 1 % P/S antibiotics. Plates were left
782 48 hours and d-luciferin (Promega #E1605; dissolved in PBS) was added to the DMEM media in
783 a concentration (150 µg/mL). Plates were then imaged using the Xenogen IVIS 200 machine
784 (PerkinElmer) and analyzed with Living Image 4.2 software.

785 The difference in the DTCs burden between the vehicle- and VPS34IN1-treated groups was
786 quantified as a foldchange difference in bioluminescence emitted signal between the two groups.
787 Foldchange values were represented in Log values and the two groups (control and drug treated)
788 were compared by a two-tailed t-test to calculate the *p*-value. The resulting values are stated on
789 the graph and in main text.

790

791 ***Ex vivo metastasis assay***. Mice were injected intraperitoneally with 150 mg/kg d-luciferin (in
792 PBS) solution and were euthanized 5-7 minutes later. Lungs were immediately collected and
793 imaged using the Xenogen IVIS 200 machine (PerkinElmer).
794

795

796 **Cell proliferation, death, and competition assays**

797

798 Detailed protocols on executing these experiments in addition to their analysis and statistical
799 tests are included in the Supplementary Methods section.

800

801 **Protein extraction, western blotting, and mTORC1 activity analyses**

802

803 Details of processing cell lysates and tumor samples for protein extraction and subsequent
804 immunoblotting are included in the Supplementary Methods section.

805

806 **RNA-Seq, Whole-genome Sequencing of 4T1-4T07 cells, and PDX15-related analyses**

807

808 Procedure of generating these datasets in addition to their analysis (thresholds, software, etc.) are
809 included in the Supplementary Methods section. Detailed description of investigating the PIK3C3
810 E562K mutation is also available in the same section.

811

812 **Clinical datasets mining and bioinformatics analysis of clinical outcome**

813

814 Details on the Single-sample Gene Set Enrichment Analysis (ssGSEA) and downstream analyses
815 are indicated in the Supplementary Methods section.

816

REFERENCES

1. H. S. McKenzie, T. Maishman, P. Simmonds, L. Durcan, P. S. Group, D. Eccles, E. Copson, Survival and disease characteristics of de novo versus recurrent metastatic breast cancer in a cohort of young patients. *Br J Cancer* **122**, 1618-1629 (2020).
2. H. Kennecke, R. Yerushalmi, R. Woods, M. C. Cheang, D. Voduc, C. H. Speers, T. O. Nielsen, K. Gelmon, Metastatic behavior of breast cancer subtypes. *J Clin Oncol* **28**, 3271-3277 (2010).
3. T. G. Karrison, D. J. Ferguson, P. Meier, Dormancy of mammary carcinoma after mastectomy. *J Natl Cancer Inst* **91**, 80-85 (1999).
4. E. Risson, A. R. Nobre, V. Maguer-Satta, J. A. Aguirre-Ghiso, The current paradigm and challenges ahead for the dormancy of disseminated tumor cells. *Nat Cancer* **1**, 672-680 (2020).
5. P. Carlson, A. Dasgupta, C. A. Grzelak, J. Kim, A. Barrett, I. M. Coleman, R. E. Shor, E. T. Goddard, J. Dai, E. M. Schweitzer, A. R. Lim, S. B. Crist, D. A. Cheresh, P. S. Nelson, K. C. Hansen, C. M. Ghajar, Targeting the perivascular niche sensitizes disseminated tumour cells to chemotherapy. *Nat Cell Biol* **21**, 238-250 (2019).
6. M. Montagner, R. Bhome, S. Hooper, P. Chakravarty, X. Qin, J. Sufi, A. Bhargava, C. D. H. Ratcliffe, Y. Naito, A. Pocaterra, C. J. Tape, E. Sahai, Crosstalk with lung epithelial cells regulates Sfrp2-mediated latency in breast cancer dissemination. *Nat Cell Biol* **22**, 289-296 (2020).
7. A. R. Nobre, E. Risson, D. K. Singh, J. S. Di Martino, J. F. Cheung, J. Wang, J. Johnson, H. G. Russnes, J. J. Bravo-Cordero, A. Birbrair, B. Naume, M. Azhar, P. S. Frenette, J. A. Aguirre-Ghiso, Bone marrow NG2(+)/Nestin(+) mesenchymal stem cells drive DTC dormancy via TGFbeta2. *Nat Cancer* **2**, 327-339 (2021).
8. I. E. Elkholi, A. Lalonde, M. Park, J. F. Cote, Breast Cancer Metastatic Dormancy and Relapse: An Enigma of Microenvironment(s). *Cancer Res* **82**, 4497-4510 (2022).
9. C. J. Aslakson, F. R. Miller, Selective events in the metastatic process defined by analysis of the sequential dissemination of subpopulations of a mouse mammary tumor. *Cancer Res* **52**, 1399-1405 (1992).
10. P. Tallon de Lara, H. Castanon, M. Vermeer, N. Nunez, K. Silina, B. Sobottka, J. Urdinez, V. Cecconi, H. Yagita, F. Movahedian Attar, S. Hiltbrunner, I. Glarner, H. Moch, S. Tugues, B. Becher, M. van den Broek, CD39(+)PD-1(+)CD8(+) T cells mediate metastatic dormancy in breast cancer. *Nat Commun* **12**, 769 (2021).
11. J. Yang, S. A. Mani, J. L. Donaher, S. Ramaswamy, R. A. Itzykson, C. Come, P. Savagner, I. Gitelman, A. Richardson, R. A. Weinberg, Twist, a master regulator of morphogenesis, plays an essential role in tumor metastasis. *Cell* **117**, 927-939 (2004).
12. H. Gao, G. Chakraborty, A. P. Lee-Lim, Q. Mo, M. Decker, A. Vonica, R. Shen, E. Brogi, A. H. Brivanlou, F. G. Giancotti, The BMP inhibitor Coco reactivates breast cancer cells at lung metastatic sites. *Cell* **150**, 764-779 (2012).
13. J. Park, R. W. Wysocki, Z. Amoozgar, L. Maiorino, M. R. Fein, J. Jorns, A. F. Schott, Y. Kinugasa-Katayama, Y. Lee, N. H. Won, E. S. Nakasone, S. A. Hearn, V. Kuttner, J. Qiu, A. S. Almeida, N. Perurena, K. Kessenbrock, M. S. Goldberg, M. Egeblad, Cancer cells induce metastasis-supporting neutrophil extracellular DNA traps. *Sci Transl Med* **8**, 361ra138 (2016).
14. T. Hart, M. Chandrashekhar, M. Aregger, Z. Steinhart, K. R. Brown, G. MacLeod, M. Mis, M. Zimmermann, A. Fradet-Turcotte, S. Sun, P. Mero, P. Dirks, S. Sidhu, F. P. Roth, O. S. Rissland, D. Durocher, S. Angers, J. Moffat, High-Resolution CRISPR Screens Reveal Fitness Genes and Genotype-Specific Cancer Liabilities. *Cell* **163**, 1515-1526 (2015).

866 15. Z. Steinhart, Z. Pavlovic, M. Chandrashekhar, T. Hart, X. Wang, X. Zhang, M. Robitaille,
867 K. R. Brown, S. Jaksani, R. Overmeer, S. F. Boj, J. Adams, J. Pan, H. Clevers, S. Sidhu, J.
868 Moffat, S. Angers, Genome-wide CRISPR screens reveal a Wnt-FZD5 signaling circuit as
869 a druggable vulnerability of RNF43-mutant pancreatic tumors. *Nat Med* **23**, 60-68 (2017).
870 16. T. Wang, H. Yu, N. W. Hughes, B. Liu, A. Kendirli, K. Klein, W. W. Chen, E. S. Lander,
871 D. M. Sabatini, Gene Essentiality Profiling Reveals Gene Networks and Synthetic Lethal
872 Interactions with Oncogenic Ras. *Cell* **168**, 890-903 e815 (2017).
873 17. M. R. Schlabach, J. Luo, N. L. Solimini, G. Hu, Q. Xu, M. Z. Li, Z. Zhao, A.
874 Smogorzewska, M. E. Sowa, X. L. Ang, T. F. Westbrook, A. C. Liang, K. Chang, J. A.
875 Hackett, J. W. Harper, G. J. Hannon, S. J. Elledge, Cancer proliferation gene discovery
876 through functional genomics. *Science* **319**, 620-624 (2008).
877 18. B. Schrors, S. Boegel, C. Albrecht, T. Bukur, V. Bukur, C. Holtstrater, C. Ritzel, K.
878 Manninen, A. D. Tadmor, M. Vormehr, U. Sahin, M. Lower, Multi-Omics
879 Characterization of the 4T1 Murine Mammary Gland Tumor Model. *Front Oncol* **10**, 1195
880 (2020).
881 19. E. H. Yau, I. R. Kummetha, G. Lichinchi, R. Tang, Y. Zhang, T. M. Rana, Genome-Wide
882 CRISPR Screen for Essential Cell Growth Mediators in Mutant KRAS Colorectal Cancers.
883 *Cancer Res* **77**, 6330-6339 (2017).
884 20. J. Joung, S. Konermann, J. S. Gootenberg, O. O. Abudayyeh, R. J. Platt, M. D. Brigham,
885 N. E. Sanjana, F. Zhang, Genome-scale CRISPR-Cas9 knockout and transcriptional
886 activation screening. *Nat Protoc* **12**, 828-863 (2017).
887 21. T. Bertomeu, J. Coulombe-Huntington, A. Chatr-Aryamontri, K. G. Bourdages, E.
888 Coyaud, B. Raught, Y. Xia, M. Tyers, A High-Resolution Genome-Wide CRISPR/Cas9
889 Viability Screen Reveals Structural Features and Contextual Diversity of the Human Cell-
890 Essential Proteome. *Mol Cell Biol* **38**, (2018).
891 22. G. MacLeod, D. A. Bozek, N. Rajakulendran, V. Monteiro, M. Ahmadi, Z. Steinhart, M.
892 M. Kushida, H. Yu, F. J. Coutinho, F. M. G. Cavalli, I. Restall, X. Hao, T. Hart, H. A.
893 Luchman, S. Weiss, P. B. Dirks, S. Angers, Genome-Wide CRISPR-Cas9 Screens Expose
894 Genetic Vulnerabilities and Mechanisms of Temozolomide Sensitivity in Glioblastoma
895 Stem Cells. *Cell Rep* **27**, 971-986 e979 (2019).
896 23. C. Fritsch, A. Huang, C. Chatenay-Rivauday, C. Schnell, A. Reddy, M. Liu, A. Kauffmann,
897 D. Guthy, D. Erdmann, A. De Pover, P. Furet, H. Gao, S. Ferretti, Y. Wang, J. Trappe, S.
898 M. Brachmann, S. M. Maira, C. Wilson, M. Boehm, C. Garcia-Echeverria, P. Chene, M.
899 Wiesmann, R. Cozens, J. Lehar, R. Schlegel, G. Caravatti, F. Hofmann, W. R. Sellers,
900 Characterization of the novel and specific PI3Kalpha inhibitor NVP-BYL719 and
901 development of the patient stratification strategy for clinical trials. *Mol Cancer Ther* **13**,
902 1117-1129 (2014).
903 24. R. Bago, N. Malik, M. J. Munson, A. R. Prescott, P. Davies, E. Sommer, N. Shpiro, R.
904 Ward, D. Cross, I. G. Ganley, D. R. Alessi, Characterization of VPS34-IN1, a selective
905 inhibitor of Vps34, reveals that the phosphatidylinositol 3-phosphate-binding SGK3
906 protein kinase is a downstream target of class III phosphoinositide 3-kinase. *Biochem J*
907 **463**, 413-427 (2014).
908 25. M. Elkabets, S. Vora, D. Juric, N. Morse, M. Mino-Kenudson, T. Muranen, J. Tao, A. B.
909 Campos, J. Rodon, Y. H. Ibrahim, V. Serra, V. Rodrik-Outmezguine, S. Hazra, S. Singh,
910 P. Kim, C. Quadt, M. Liu, A. Huang, N. Rosen, J. A. Engelman, M. Scaltriti, J. Baselga,
911 mTORC1 inhibition is required for sensitivity to PI3K p110alpha inhibitors in PIK3CA-
912 mutant breast cancer. *Sci Transl Med* **5**, 196ra199 (2013).
913 26. R. A. Saxton, D. M. Sabatini, mTOR Signaling in Growth, Metabolism, and Disease. *Cell*
914 **169**, 361-371 (2017).

915 27. R. Bago, E. Sommer, P. Castel, C. Crafter, F. P. Bailey, N. Shpiro, J. Baselga, D. Cross, P.
916 A. Eyers, D. R. Alessi, The hVps34-SGK3 pathway alleviates sustained PI3K/Akt
917 inhibition by stimulating mTORC1 and tumour growth. *EMBO J* **35**, 2263 (2016).
918 28. D. M. Schewe, J. A. Aguirre-Ghiso, ATF6alpha-Rheb-mTOR signaling promotes survival
919 of dormant tumor cells in vivo. *Proc Natl Acad Sci U S A* **105**, 10519-10524 (2008).
920 29. Y. Zhang, P. Kwok-Shing Ng, M. Kucherlapati, F. Chen, Y. Liu, Y. H. Tsang, G. de
921 Velasco, K. J. Jeong, R. Akbani, A. Hadjipanayis, A. Pantazi, C. A. Bristow, E. Lee, H. S.
922 Mahadeshwar, J. Tang, J. Zhang, L. Yang, S. Seth, S. Lee, X. Ren, X. Song, H. Sun, J.
923 Seidman, L. J. Luquette, R. Xi, L. Chin, A. Protopopov, T. F. Westbrook, C. S. Shelley, T.
924 K. Choueiri, M. Ittmann, C. Van Waes, J. N. Weinstein, H. Liang, E. P. Henske, A. K.
925 Godwin, P. J. Park, R. Kucherlapati, K. L. Scott, G. B. Mills, D. J. Kwiatkowski, C. J.
926 Creighton, A Pan-Cancer Proteogenomic Atlas of PI3K/AKT/mTOR Pathway Alterations.
927 *Cancer Cell* **31**, 820-832 e823 (2017).
928 30. C. G. Fedele, L. M. Ooms, M. Ho, J. Vieusseux, S. A. O'Toole, E. K. Millar, E. Lopez-
929 Knowles, A. Sriratana, R. Gurung, L. Baglietto, G. G. Giles, C. G. Bailey, J. E. Rasko, B.
930 J. Shields, J. T. Price, P. W. Majerus, R. L. Sutherland, T. Tiganis, C. A. McLean, C. A.
931 Mitchell, Inositol polyphosphate 4-phosphatase II regulates PI3K/Akt signaling and is lost
932 in human basal-like breast cancers. *Proc Natl Acad Sci U S A* **107**, 22231-22236 (2010).
933 31. H. Liu, M. N. Paddock, H. Wang, C. J. Murphy, R. C. Geck, A. J. Navarro, G. M. Wulf,
934 O. Elemento, V. Haucke, L. C. Cantley, A. Toker, The INPP4B Tumor Suppressor
935 Modulates EGFR Trafficking and Promotes Triple-Negative Breast Cancer. *Cancer*
936 *Discov* **10**, 1226-1239 (2020).
937 32. T. Nobukuni, M. Joaquin, M. Roccio, S. G. Dann, S. Y. Kim, P. Gulati, M. P. Byfield, J.
938 M. Backer, F. Natt, J. L. Bos, F. J. Zwartkruis, G. Thomas, Amino acids mediate
939 mTOR/raptor signaling through activation of class 3 phosphatidylinositol 3OH-kinase.
940 *Proc Natl Acad Sci U S A* **102**, 14238-14243 (2005).
941 33. M. P. Byfield, J. T. Murray, J. M. Backer, hVps34 is a nutrient-regulated lipid kinase
942 required for activation of p70 S6 kinase. *J Biol Chem* **280**, 33076-33082 (2005).
943 34. Z. Hong, N. M. Pedersen, L. Wang, M. L. Torgersen, H. Stenmark, C. Raiborg, PtdIns3P
944 controls mTORC1 signaling through lysosomal positioning. *J Cell Biol* **216**, 4217-4233
945 (2017).
946 35. V. I. Korolchuk, S. Saiki, M. Lichtenberg, F. H. Siddiqi, E. A. Roberts, S. Imarisio, L.
947 Jahreiss, S. Sarkar, M. Futter, F. M. Menzies, C. J. O'Kane, V. Deretic, D. C. Rubinsztein,
948 Lysosomal positioning coordinates cellular nutrient responses. *Nat Cell Biol* **13**, 453-460
949 (2011).
950 36. J. Copp, G. Manning, T. Hunter, TORC-specific phosphorylation of mammalian target of
951 rapamycin (mTOR): phospho-Ser2481 is a marker for intact mTOR signaling complex 2.
952 *Cancer Res* **69**, 1821-1827 (2009).
953 37. Y. Sancak, T. R. Peterson, Y. D. Shaul, R. A. Lindquist, C. C. Thoreen, L. Bar-Peled, D.
954 M. Sabatini, The Rag GTPases bind raptor and mediate amino acid signaling to mTORC1.
955 *Science* **320**, 1496-1501 (2008).
956 38. C. Betz, M. N. Hall, Where is mTOR and what is it doing there? *J Cell Biol* **203**, 563-574
957 (2013).
958 39. M. Rosner, M. Hengstschlager, Cytoplasmic and nuclear distribution of the protein
959 complexes mTORC1 and mTORC2: rapamycin triggers dephosphorylation and
960 delocalization of the mTORC2 components rictor and sin1. *Hum Mol Genet* **17**, 2934-2948
961 (2008).
962 40. P. Savage, A. Pacis, H. Kuasne, L. Liu, D. Lai, A. Wan, M. Dankner, C. Martinez, V.
963 Munoz-Ramos, V. Pilon, A. Monast, H. Zhao, M. Souleimanova, M. G. Annis, A. Aguilar-
964 Mahecha, J. Lafleur, N. R. Bertos, J. Asselah, N. Bouganim, K. Petrecca, P. M. Siegel, A.

965 Omeroglu, S. P. Shah, S. Aparicio, M. Basik, S. Meterissian, M. Park, Chemogenomic
966 profiling of breast cancer patient-derived xenografts reveals targetable vulnerabilities for
967 difficult-to-treat tumors. *Commun Biol* **3**, 310 (2020).
968 41. M. J. Munson, G. F. Allen, R. Toth, D. G. Campbell, J. M. Lucocq, I. G. Ganley, mTOR
969 activates the VPS34-UVRAG complex to regulate autolysosomal tubulation and cell
970 survival. *EMBO J* **34**, 2272-2290 (2015).
971 42. J. A. van der Hage, L. J. van den Broek, C. Legrand, P. C. Clahsen, C. J. Bosch, E. C.
972 Robanus-Maandag, C. J. van de Velde, M. J. van de Vijver, Overexpression of P70 S6
973 kinase protein is associated with increased risk of locoregional recurrence in node-negative
974 premenopausal early breast cancer patients. *Br J Cancer* **90**, 1543-1550 (2004).
975 43. A. Liberzon, C. Birger, H. Thorvaldsdottir, M. Ghandi, J. P. Mesirov, P. Tamayo, The
976 Molecular Signatures Database (MSigDB) hallmark gene set collection. *Cell Syst* **1**, 417-
977 425 (2015).
978 44. T. Tian, X. Li, J. Zhang, mTOR Signaling in Cancer and mTOR Inhibitors in Solid Tumor
979 Targeting Therapy. *Int J Mol Sci* **20**, (2019).
980 45. C. A. Grzelak, E. T. Goddard, E. E. Lederer, K. Rajaram, J. Dai, R. E. Shor, A. R. Lim, J.
981 Kim, S. Beronja, A. P. W. Funnell, C. M. Ghajar, Elimination of fluorescent protein
982 immunogenicity permits modeling of metastasis in immune-competent settings. *Cancer*
983 *Cell*, (2021).
984 46. L. M. Balz, K. Bartkowiak, A. Andreas, K. Pantel, B. Niggemann, K. S. Zanker, B. H.
985 Brandt, T. Dittmar, The interplay of HER2/HER3/PI3K and EGFR/HER2/PLC-gamma1
986 signalling in breast cancer cell migration and dissemination. *J Pathol* **227**, 234-244 (2012).
987 47. L. Vera-Ramirez, S. K. Vodnala, R. Nini, K. W. Hunter, J. E. Green, Autophagy promotes
988 the survival of dormant breast cancer cells and metastatic tumour recurrence. *Nat Commun*
989 **9**, 1944 (2018).
990 48. A. La Belle Flynn, B. C. Calhoun, A. Sharma, J. C. Chang, A. Almasan, W. P. Schiemann,
991 Autophagy inhibition elicits emergence from metastatic dormancy by inducing and
992 stabilizing Pfkfb3 expression. *Nat Commun* **10**, 3668 (2019).
993 49. M. S. Yoon, G. Du, J. M. Backer, M. A. Frohman, J. Chen, Class III PI-3-kinase activates
994 phospholipase D in an amino acid-sensing mTORC1 pathway. *J Cell Biol* **195**, 435-447
995 (2011).
996 50. A. P. Mutvei, M. J. Nagiec, J. C. Hamann, S. G. Kim, C. T. Vincent, J. Blenis, Rap1-
997 GTPases control mTORC1 activity by coordinating lysosome organization with amino
998 acid availability. *Nat Commun* **11**, 1416 (2020).
999 51. L. Yu, C. K. McPhee, L. Zheng, G. A. Mardones, Y. Rong, J. Peng, N. Mi, Y. Zhao, Z.
000 Liu, F. Wan, D. W. Hailey, V. Oorschot, J. Klumperman, E. H. Baehrecke, M. J. Lenardo,
001 Termination of autophagy and reformation of lysosomes regulated by mTOR. *Nature* **465**,
002 942-946 (2010).
003 52. R. E. Shor, J. Dai, S. Y. Lee, L. Pisarsky, I. Matei, S. Lucotti, D. Lyden, M. J. Bissell, C.
004 M. Ghajar, The PI3K/mTOR inhibitor Gedatolisib eliminates dormant breast cancer cells
005 in organotypic culture, but fails to prevent metastasis in preclinical settings. *Mol Oncol* **16**,
006 130-147 (2022).
007 53. V. Ponomarev, M. Doubrovin, I. Serganova, J. Vider, A. Shavrin, T. Beresten, A. Ivanova,
008 L. Ageyeva, V. Tourkova, J. Balatoni, W. Bornmann, R. Blasberg, J. Gelovani Tjuvajev,
009 A novel triple-modality reporter gene for whole-body fluorescent, bioluminescent, and
010 nuclear noninvasive imaging. *Eur J Nucl Med Mol Imaging* **31**, 740-751 (2004).
011 54. W. Li, J. Koster, H. Xu, C. H. Chen, T. Xiao, J. S. Liu, M. Brown, X. S. Liu, Quality
012 control, modeling, and visualization of CRISPR screens with MAGeCK-VISPR. *Genome*
013 *Biol* **16**, 281 (2015).

014 55. T. Hart, K. R. Brown, F. Sircoulomb, R. Rottapel, J. Moffat, Measuring error rates in
015 genomic perturbation screens: gold standards for human functional genomics. *Mol Syst*
016 *Biol* **10**, 733 (2014).
017 56. T. Hart, J. Moffat, BAGEL: a computational framework for identifying essential genes
018 from pooled library screens. *BMC Bioinformatics* **17**, 164 (2016).
019 57. T. Hart, A. H. Y. Tong, K. Chan, J. Van Leeuwen, A. Seetharaman, M. Aregger, M.
020 Chandrashekhar, N. Hustedt, S. Seth, A. Noonan, A. Habsid, O. Sizova, L. Nedyalkova,
021 R. Climie, L. Tworzyanski, K. Lawson, M. A. Sartori, S. Alibeh, D. Tieu, S. Masud, P.
022 Mero, A. Weiss, K. R. Brown, M. Usaj, M. Billmann, M. Rahman, M. Constanzo, C. L.
023 Myers, B. J. Andrews, C. Boone, D. Durocher, J. Moffat, Evaluation and Design of
024 Genome-Wide CRISPR/SpCas9 Knockout Screens. *G3 (Bethesda)* **7**, 2719-2727 (2017).
025 58. A. Robert, P. Tian, S. A. Adam, M. Kittisopikul, K. Jaqaman, R. D. Goldman, V. I.
026 Gelfand, Kinesin-dependent transport of keratin filaments: a unified mechanism for
027 intermediate filament transport. *FASEB J* **33**, 388-399 (2019).
028 59. https://www.bioinformatics.babraham.ac.uk/projects/fastqc/.
029 60. C. Trapnell, A. Roberts, L. Goff, G. Pertea, D. Kim, D. R. Kelley, H. Pimentel, S. L.
030 Salzberg, J. L. Rinn, L. Pachter, Differential gene and transcript expression analysis of
031 RNA-seq experiments with TopHat and Cufflinks. *Nat Protoc* **7**, 562-578 (2012).
032 61. Y. Liao, G. K. Smyth, W. Shi, featureCounts: an efficient general purpose program for
033 assigning sequence reads to genomic features. *Bioinformatics* **30**, 923-930 (2014).
034 62. S. Anders, W. Huber, Differential expression analysis for sequence count data. *Genome*
035 *Biol* **11**, R106 (2010).
036 63. M. Ashburner, C. A. Ball, J. A. Blake, D. Botstein, H. Butler, J. M. Cherry, A. P. Davis,
037 K. Dolinski, S. S. Dwight, J. T. Eppig, M. A. Harris, D. P. Hill, L. Issel-Tarver, A.
038 Kasarskis, S. Lewis, J. C. Matese, J. E. Richardson, M. Ringwald, G. M. Rubin, G.
039 Sherlock, Gene ontology: tool for the unification of biology. The Gene Ontology
040 Consortium. *Nat Genet* **25**, 25-29 (2000).
041 64. C. Gene Ontology, The Gene Ontology resource: enriching a GOld mine. *Nucleic Acids*
042 *Res* **49**, D325-D334 (2021).
043 65. V. K. Mootha, C. M. Lindgren, K. F. Eriksson, A. Subramanian, S. Sihag, J. Lehar, P.
044 Puigserver, E. Carlsson, M. Ridderstrale, E. Laurila, N. Houstis, M. J. Daly, N. Patterson,
045 J. P. Mesirov, T. R. Golub, P. Tamayo, B. Spiegelman, E. S. Lander, J. N. Hirschhorn, D.
046 Altshuler, L. C. Groop, PGC-1alpha-responsive genes involved in oxidative
047 phosphorylation are coordinately downregulated in human diabetes. *Nat Genet* **34**, 267-
048 273 (2003).
049 66. A. Subramanian, P. Tamayo, V. K. Mootha, S. Mukherjee, B. L. Ebert, M. A. Gillette, A.
050 Paulovich, S. L. Pomeroy, T. R. Golub, E. S. Lander, J. P. Mesirov, Gene set enrichment
051 analysis: a knowledge-based approach for interpreting genome-wide expression profiles.
052 *Proc Natl Acad Sci U S A* **102**, 15545-15550 (2005).
053 67. C. Klijn, S. Durinck, E. W. Stawiski, P. M. Haverty, Z. Jiang, H. Liu, J. Degenhardt, O.
054 Mayba, F. Gnad, J. Liu, G. Pau, J. Reeder, Y. Cao, K. Mukhyala, S. K. Selvaraj, M. Yu,
055 G. J. Zynda, M. J. Brauer, T. D. Wu, R. C. Gentleman, G. Manning, R. L. Yauch, R.
056 Bourgon, D. Stokoe, Z. Modrusan, R. M. Neve, F. J. de Sauvage, J. Settleman, S. Seshagiri,
057 Z. Zhang, A comprehensive transcriptional portrait of human cancer cell lines. *Nat*
058 *Biotechnol* **33**, 306-312 (2015).
059 68. S. Durinck, P. T. Spellman, E. Birney, W. Huber, Mapping identifiers for the integration
060 of genomic datasets with the R/Bioconductor package biomaRt. *Nat Protoc* **4**, 1184-1191
061 (2009).
062 69. M. Ghandi, F. W. Huang, J. Jane-Valbuena, G. V. Kryukov, C. C. Lo, E. R. McDonald,
063 3rd, J. Barretina, E. T. Gelfand, C. M. Bielski, H. Li, K. Hu, A. Y. Andreev-Drakhlin, J.

Kim, J. M. Hess, B. J. Haas, F. Aguet, B. A. Weir, M. V. Rothberg, B. R. Paolella, M. S. Lawrence, R. Akbani, Y. Lu, H. L. Tiv, P. C. Gokhale, A. de Weck, A. A. Mansour, C. Oh, J. Shih, K. Hadi, Y. Rosen, J. Bistline, K. Venkatesan, A. Reddy, D. Sonkin, M. Liu, J. Lehar, J. M. Korn, D. A. Porter, M. D. Jones, J. Golji, G. Caponigro, J. E. Taylor, C. M. Dunning, A. L. Creech, A. C. Warren, J. M. McFarland, M. Zamanighomi, A. Kauffmann, N. Stransky, M. Imielinski, Y. E. Maruvka, A. D. Cherniack, A. Tsherniak, F. Vazquez, J. D. Jaffe, A. A. Lane, D. M. Weinstock, C. M. Johannessen, M. P. Morrissey, F. Stegmeier, R. Schlegel, W. C. Hahn, G. Getz, G. B. Mills, J. S. Boehm, T. R. Golub, L. A. Garraway, W. R. Sellers, Next-generation characterization of the Cancer Cell Line Encyclopedia. *Nature* **569**, 503-508 (2019).

70. R. M. Neve, K. Chin, J. Fridlyand, J. Yeh, F. L. Baehner, T. Fevr, L. Clark, N. Bayani, J. P. Coppe, F. Tong, T. Speed, P. T. Spellman, S. DeVries, A. Lapuk, N. J. Wang, W. L. Kuo, J. L. Stilwell, D. Pinkel, D. G. Albertson, F. M. Waldman, F. McCormick, R. B. Dickson, M. D. Johnson, M. Lippman, S. Ethier, A. Gazdar, J. W. Gray, A collection of breast cancer cell lines for the study of functionally distinct cancer subtypes. *Cancer Cell* **10**, 515-527 (2006).

71. H. Jiang, R. Lei, S. W. Ding, S. Zhu, Skewer: a fast and accurate adapter trimmer for next-generation sequencing paired-end reads. *BMC Bioinformatics* **15**, 182 (2014).

72. H. Li, R. Durbin, Fast and accurate short read alignment with Burrows-Wheeler transform. *Bioinformatics* **25**, 1754-1760 (2009).

73. F. Favero, T. Joshi, A. M. Marquard, N. J. Birkbak, M. Krzystanek, Q. Li, Z. Szallasi, A. C. Eklund, Sequenza: allele-specific copy number and mutation profiles from tumor sequencing data. *Ann Oncol* **26**, 64-70 (2015).

74. K. Cibulskis, M. S. Lawrence, S. L. Carter, A. Sivachenko, D. Jaffe, C. Sougnez, S. Gabriel, M. Meyerson, E. S. Lander, G. Getz, Sensitive detection of somatic point mutations in impure and heterogeneous cancer samples. *Nat Biotechnol* **31**, 213-219 (2013).

75. R. M. Layer, C. Chiang, A. R. Quinlan, I. M. Hall, LUMPY: a probabilistic framework for structural variant discovery. *Genome Biol* **15**, R84 (2014).

76. P. Cingolani, A. Platts, L. Wang le, M. Coon, T. Nguyen, L. Wang, S. J. Land, X. Lu, D. M. Ruden, A program for annotating and predicting the effects of single nucleotide polymorphisms, SnpEff: SNPs in the genome of Drosophila melanogaster strain w1118; iso-2; iso-3. *Fly (Austin)* **6**, 80-92 (2012).

77. A. M. Bolger, M. Lohse, B. Usadel, Trimmomatic: a flexible trimmer for Illumina sequence data. *Bioinformatics* **30**, 2114-2120 (2014).

78. A. Dobin, C. A. Davis, F. Schlesinger, J. Drenkow, C. Zaleski, S. Jha, P. Batut, M. Chaisson, T. R. Gingeras, STAR: ultrafast universal RNA-seq aligner. *Bioinformatics* **29**, 15-21 (2013).

79. M. I. Love, W. Huber, S. Anders, Moderated estimation of fold change and dispersion for RNA-seq data with DESeq2. *Genome Biol* **15**, 550 (2014).

80. H. Li, B. Handsaker, A. Wysoker, T. Fennell, J. Ruan, N. Homer, G. Marth, G. Abecasis, R. Durbin, S. Genome Project Data Processing, The Sequence Alignment/Map format and SAMtools. *Bioinformatics* **25**, 2078-2079 (2009).

81. A. R. Quinlan, I. M. Hall, BEDTools: a flexible suite of utilities for comparing genomic features. *Bioinformatics* **26**, 841-842 (2010).

82. S. Nahle, L. Quirion, J. Boulais, H. Bagci, D. Faubert, A. C. Gingras, J. F. Cote, Defining the interactomes of proteins involved in cytoskeletal dynamics using high-throughput proximity-dependent biotinylation in cellulo. *STAR Protoc* **3**, 101075 (2022).

83. K. L. Bolton, R. N. Ptashkin, T. Gao, L. Braunstein, S. M. Devlin, D. Kelly, M. Patel, A. Berthon, A. Syed, M. Yabe, C. C. Coombs, N. M. Caltabellotta, M. Walsh, K. Offit, Z.

Stadler, D. Mandelker, J. Schulman, A. Patel, J. Philip, E. Bernard, G. Gundem, J. E. A. Ossa, M. Levine, J. S. M. Martinez, N. Farnoud, D. Glodzik, S. Li, M. E. Robson, C. Lee, P. D. P. Pharoah, K. H. Stopsack, B. Spitzer, S. Mantha, J. Fagin, L. Boucai, C. J. Gibson, B. L. Ebert, A. L. Young, T. Druley, K. Takahashi, N. Gillis, M. Ball, E. Padron, D. M. Hyman, J. Baselga, L. Norton, S. Gardos, V. M. Klimek, H. Scher, D. Bajorin, E. Paraiso, R. Benayed, M. E. Arcila, M. Ladanyi, D. B. Solit, M. F. Berger, M. Tallman, M. Garcia-Closas, N. Chatterjee, L. A. Diaz, Jr., R. L. Levine, L. M. Morton, A. Zehir, E. Papaemmanuil, Cancer therapy shapes the fitness landscape of clonal hematopoiesis. *Nat Genet* **52**, 1219-1226 (2020).

84. I. T. P.-C. A. o. W. G. Consortium, Pan-cancer analysis of whole genomes. *Nature* **578**, 82-93 (2020).

85. D. M. Hyman, S. A. Piha-Paul, H. Won, J. Rodon, C. Saura, G. I. Shapiro, D. Juric, D. I. Quinn, V. Moreno, B. Doger, I. A. Mayer, V. Boni, E. Calvo, S. Loi, A. C. Lockhart, J. P. Erinjeri, M. Scaltriti, G. A. Ulaner, J. Patel, J. Tang, H. Beer, S. D. Selcuklu, A. J. Hanrahan, N. Bouvier, M. Melcer, R. Murali, A. M. Schram, L. M. Smyth, K. Jhaveri, B. T. Li, A. Drilon, J. J. Harding, G. Iyer, B. S. Taylor, M. F. Berger, R. E. Cutler, Jr., F. Xu, A. Butturini, L. D. Eli, G. Mann, C. Farrell, A. S. Lalani, R. P. Bryce, C. L. Arteaga, F. Meric-Bernstam, J. Baselga, D. B. Solit, HER kinase inhibition in patients with HER2- and HER3-mutant cancers. *Nature* **554**, 189-194 (2018).

86. D. Miao, C. A. Margolis, N. I. Vokes, D. Liu, A. Taylor-Weiner, S. M. Wankowicz, D. Adeegbe, D. Keliher, B. Schilling, A. Tracy, M. Manos, N. G. Chau, G. J. Hanna, P. Polak, S. J. Rodig, S. Signoretti, L. M. Sholl, J. A. Engelman, G. Getz, P. A. Janne, R. I. Haddad, T. K. Choueiri, D. A. Barbie, R. Haq, M. M. Awad, D. Schadendorf, F. S. Hodi, J. Bellmunt, K. K. Wong, P. Hammerman, E. M. Van Allen, Genomic correlates of response to immune checkpoint blockade in microsatellite-stable solid tumors. *Nat Genet* **50**, 1271-1281 (2018).

87. B. Nguyen, C. Fong, A. Luthra, S. A. Smith, R. G. DiNatale, S. Nandakumar, H. Walch, W. K. Chatila, R. Madupuri, R. Kundra, C. M. Bielski, B. Mastrogiacomo, M. T. A. Donoghue, A. Boire, S. Chandarlapaty, K. Ganesh, J. J. Harding, C. A. Iacobuzio-Donahue, P. Razavi, E. Reznik, C. M. Rudin, D. Zamarin, W. Abida, G. K. Abou-Alfa, C. Aghajanian, A. Cercek, P. Chi, D. Feldman, A. L. Ho, G. Iyer, Y. Y. Janjigian, M. Morris, R. J. Motzer, E. M. O'Reilly, M. A. Postow, N. P. Raj, G. J. Riely, M. E. Robson, J. E. Rosenberg, A. Safonov, A. N. Shoushtari, W. Tap, M. Y. Teo, A. M. Varghese, M. Voss, R. Yaeger, M. G. Zauderer, N. Abu-Rustum, J. Garcia-Aguilar, B. Bochner, A. Hakimi, W. R. Jarnagin, D. R. Jones, D. Molena, L. Morris, E. Rios-Doria, P. Russo, S. Singer, V. E. Strong, D. Chakravarty, L. H. Ellenson, A. Gopalan, J. S. Reis-Filho, B. Weigelt, M. Ladanyi, M. Gonen, S. P. Shah, J. Massague, J. Gao, A. Zehir, M. F. Berger, D. B. Solit, S. F. Bakhoum, F. Sanchez-Vega, N. Schultz, Genomic characterization of metastatic patterns from prospective clinical sequencing of 25,000 patients. *Cell* **185**, 563-575 e511 (2022).

88. D. R. Robinson, Y. M. Wu, R. J. Lonigro, P. Vats, E. Cobain, J. Everett, X. Cao, E. Rabban, C. Kumar-Sinha, V. Raymond, S. Schuetze, A. Alva, J. Siddiqui, R. Chugh, F. Worden, M. M. Zalupski, J. Innis, R. J. Mody, S. A. Tomlins, D. Lucas, L. H. Baker, N. Ramnath, A. F. Schott, D. F. Hayes, J. Vijai, K. Offit, E. M. Stoffel, J. S. Roberts, D. C. Smith, L. P. Kunju, M. Talpaz, M. Cieslik, A. M. Chinnaiyan, Integrative clinical genomics of metastatic cancer. *Nature* **548**, 297-303 (2017).

89. E. Y. Rosen, D. A. Goldman, J. F. Hechtman, R. Benayed, A. M. Schram, E. Cocco, S. Shifman, Y. Gong, R. Kundra, J. P. Solomon, A. Bardelli, M. Scaltriti, A. Drilon, A. Iasonos, B. S. Taylor, D. M. Hyman, TRK Fusions Are Enriched in Cancers with

Uncommon Histologies and the Absence of Canonical Driver Mutations. *Clin Cancer Res* **26**, 1624-1632 (2020).

90. R. M. Samstein, C. H. Lee, A. N. Shoushtari, M. D. Hellmann, R. Shen, Y. Y. Janjigian, D. A. Barron, A. Zehir, E. J. Jordan, A. Omuro, T. J. Kaley, S. M. Kendall, R. J. Motzer, A. A. Hakimi, M. H. Voss, P. Russo, J. Rosenberg, G. Iyer, B. H. Bochner, D. F. Bajorin, H. A. Al-Ahmadie, J. E. Chaft, C. M. Rudin, G. J. Riely, S. Baxi, A. L. Ho, R. J. Wong, D. G. Pfister, J. D. Wolchok, C. A. Barker, P. H. Gutin, C. W. Brennan, V. Tabar, I. K. Mellinghoff, L. M. DeAngelis, C. E. Ariyan, N. Lee, W. D. Tap, M. M. Gounder, S. P. D'Angelo, L. Saltz, Z. K. Stadler, H. I. Scher, J. Baselga, P. Razavi, C. A. Klebanoff, R. Yaeger, N. H. Segal, G. Y. Ku, R. P. DeMatteo, M. Ladanyi, N. A. Rizvi, M. F. Berger, N. Riaz, D. B. Solit, T. A. Chan, L. G. T. Morris, Tumor mutational load predicts survival after immunotherapy across multiple cancer types. *Nat Genet* **51**, 202-206 (2019).

91. L. Wu, H. Yao, H. Chen, A. Wang, K. Guo, W. Gou, Y. Yu, X. Li, M. Yao, S. Yuan, F. Pang, J. Hu, L. Chen, W. Liu, J. Yao, S. Zhang, X. Dong, W. Wang, J. Hu, Q. Ling, S. Ding, Y. Wei, Q. Li, W. Cao, S. Wang, Y. Di, F. Feng, G. Zhao, J. Zhang, L. Huang, J. Xu, W. Yan, Z. Tong, D. Jiang, T. Ji, Q. Li, L. Xu, H. He, L. Shang, J. Liu, K. Wang, D. Wu, J. Shen, Y. Liu, T. Zhang, C. Liang, Y. Wang, Y. Shang, J. Guo, G. Liang, S. Xu, J. Liu, K. Wang, M. Wang, Landscape of somatic alterations in large-scale solid tumors from an Asian population. *Nat Commun* **13**, 4264 (2022).

92. A. Zehir, R. Benayed, R. H. Shah, A. Syed, S. Middha, H. R. Kim, P. Srinivasan, J. Gao, D. Chakravarty, S. M. Devlin, M. D. Hellmann, D. A. Barron, A. M. Schram, M. Hameed, S. Dogan, D. S. Ross, J. F. Hechtman, D. F. DeLair, J. Yao, D. L. Mandelker, D. T. Cheng, R. Chandramohan, A. S. Mohanty, R. N. Ptashkin, G. Jayakumaran, M. Prasad, M. H. Syed, A. B. Rema, Z. Y. Liu, K. Nafa, L. Borsu, J. Sadowska, J. Casanova, R. Bacares, I. J. Kiecka, A. Razumova, J. B. Son, L. Stewart, T. Baldi, K. A. Mullaney, H. Al-Ahmadie, E. Vakiani, A. A. Abeshouse, A. V. Penson, P. Jonsson, N. Camacho, M. T. Chang, H. H. Won, B. E. Gross, R. Kundra, Z. J. Heins, H. W. Chen, S. Phillips, H. Zhang, J. Wang, A. Ochoa, J. Wills, M. Eubank, S. B. Thomas, S. M. Gardos, D. N. Reales, J. Galle, R. Durany, R. Cambria, W. Abida, A. Cercek, D. R. Feldman, M. M. Gounder, A. A. Hakimi, J. J. Harding, G. Iyer, Y. Y. Janjigian, E. J. Jordan, C. M. Kelly, M. A. Lowery, L. G. T. Morris, A. M. Omuro, N. Raj, P. Razavi, A. N. Shoushtari, N. Shukla, T. E. Soumerai, A. M. Varghese, R. Yaeger, J. Coleman, B. Bochner, G. J. Riely, L. B. Saltz, H. I. Scher, P. J. Sabbatini, M. E. Robson, D. S. Klimstra, B. S. Taylor, J. Baselga, N. Schultz, D. M. Hyman, M. E. Arcila, D. B. Solit, M. Ladanyi, M. F. Berger, Mutational landscape of metastatic cancer revealed from prospective clinical sequencing of 10,000 patients. *Nat Med* **23**, 703-713 (2017).

93. E. Cerami, J. Gao, U. Dogrusoz, B. E. Gross, S. O. Sumer, B. A. Aksoy, A. Jacobsen, C. J. Byrne, M. L. Heuer, E. Larsson, Y. Antipin, B. Reva, A. P. Goldberg, C. Sander, N. Schultz, The cBio cancer genomics portal: an open platform for exploring multidimensional cancer genomics data. *Cancer Discov* **2**, 401-404 (2012).

94. J. Gao, B. A. Aksoy, U. Dogrusoz, G. Dresdner, B. Gross, S. O. Sumer, Y. Sun, A. Jacobsen, R. Sinha, E. Larsson, E. Cerami, C. Sander, N. Schultz, Integrative analysis of complex cancer genomics and clinical profiles using the cBioPortal. *Sci Signal* **6**, pl1 (2013).

95. D. A. Barbie, P. Tamayo, J. S. Boehm, S. Y. Kim, S. E. Moody, I. F. Dunn, A. C. Schinzel, P. Sandy, E. Meylan, C. Scholl, S. Frohling, E. M. Chan, M. L. Sos, K. Michel, C. Mermel, S. J. Silver, B. A. Weir, J. H. Reiling, Q. Sheng, P. B. Gupta, R. C. Wadlow, H. Le, S. Hoersch, B. S. Wittner, S. Ramaswamy, D. M. Livingston, D. M. Sabatini, M. Meyerson, R. K. Thomas, E. S. Lander, J. P. Mesirov, D. E. Root, D. G. Gilliland, T. Jacks, W. C.

212 Hahn, Systematic RNA interference reveals that oncogenic KRAS-driven cancers require
213 TBK1. *Nature* **462**, 108-112 (2009).
214 96. M. Reich, T. Liefeld, J. Gould, J. Lerner, P. Tamayo, J. P. Mesirov, GenePattern 2.0. *Nat*
215 *Genet* **38**, 500-501 (2006).
216 97. N. Cancer Genome Atlas, Comprehensive molecular portraits of human breast tumours.
217 *Nature* **490**, 61-70 (2012).
218 98. C. Curtis, S. P. Shah, S. F. Chin, G. Turashvili, O. M. Rueda, M. J. Dunning, D. Speed, A.
219 G. Lynch, S. Samarajiwa, Y. Yuan, S. Graf, G. Ha, G. Haffari, A. Bashashati, R. Russell,
220 S. McKinney, M. Group, A. Langerod, A. Green, E. Provenzano, G. Wishart, S. Pinder, P.
221 Watson, F. Markowetz, L. Murphy, I. Ellis, A. Purushotham, A. L. Borresen-Dale, J. D.
222 Brenton, S. Tavare, C. Caldas, S. Aparicio, The genomic and transcriptomic architecture
223 of 2,000 breast tumours reveals novel subgroups. *Nature* **486**, 346-352 (2012).
224 99. E. R. Paquet, M. T. Hallett, Absolute assignment of breast cancer intrinsic molecular
225 subtype. *J Natl Cancer Inst* **107**, 357 (2015).
226

ACKNOWLEDGMENTS

We would like to thank Dr. Marie-Anne Goyette for providing feedbacks on the manuscript. We thank Dr. Filippo Giancotti for providing the 4T07-TGL cell line and Dr. Vladimir Ponomarev for providing the TGL reporter. We thank Drs. Sandra Turcotte, Philippe Roux, and Matthew Smith for fruitful discussions, Drs Anne-Marie Fortier and Deepak Singh for expert advice. We acknowledge the "Genome Engineering using CRISPR/Cas Systems" Google discussion group, Dr. Julia Joung, and Dr. Jonathan Boulais for helpful discussions on technical steps or the bioinformatic analysis of the CRISPR screens. We express our gratitude to the IRCM facilities staff (Dr. Dominic Filion, Manon Laprise, and Dr. Odile Neyret) for their critical technical help involved in this work.

FUNDING

This work was supported by operating grants from the Cancer Research Society (operating grant #25244 to J.-F.C), Canadian Institutes of Health Research (CIHR) (Foundation grant #FDN-143281 to M.P. and operating grant #PJT-156086 to C.L.K), Canadian Cancer Society and Oncopole grants (to M.P.) and an American Cancer Society Research Scholar Award (RSG-22-164-01-MM to A.P.G.). PDX cell lines were obtained from the breast tissue bank at McGill University, supported by grants to the Reseau Cancer banque de tumeurs from the Fonds de la Recherche du Québec- en Santé (FRQS) and the Quebec Breast Cancer Foundation (to M.P). Data computational analyses were enabled by compute and storage resources provided by Compute Canada and Calcul Québec. I.E.E. was a recipient of an FRQS Doctoral Scholarship and an IRCM Foundation-TD scholarship. S.D. is a recipient of a Miles for Moffitt postdoctoral fellowship. C.L.K. is the recipient of an FRQS Salary Award. M.P. is a Distinguished James McGill Professor and holds the Diane and Sal Guerrera Chair in Cancer Genetics. J.-F.C. holds the Canada Research Chair Tier 1 in Signalling in Cancer and Metastasis, the Alain Fontaine Chair in Cancer Research, and the Transat Chair in Breast Cancer from the IRCM Foundation.

AUTHOR CONTRIBUTIONS

Conceptualization, Supervision, Writing-Finalizing the manuscript: IEE and J-FC
Methodology & Investigation: IEE, AR, HK, SD, GM, SH, AP, VC
Formal analysis & Writing - Review & Editing: all authors
Writing—original draft: IEE

COMPETING INTEREST:

Julio Aguirre-Ghiso is a scientific co-founder, scientific advisory board member and equity owner in HiberCell and receives financial compensation as a consultant for HiberCell, a Mount Sinai spin-off company focused on the research and development of therapeutics that prevent or delay the recurrence of cancer. The remaining authors declare no competing interests.

DATA AND MATERIALS AVAILABILITY

All data are available in the main text or the supplementary materials. RNA-Seq related datasets/analyses (e.g., 4T1-4T07 differentially expressed genes and correlation with human breast cancer cell lines) are included in tables S1 and S8. Moreover, the raw data of the RNA-Seq dataset is deposited online (GSE203296) and will be publicly available starting December 1st, 2023. CRISPR screens' data are provided in tables S2-5. WGS datasets are provided in tables S6-7.